



Article

# Further Generalization and Approximation of Fractional-Order Filters and Their Inverse Functions of the Second-Order Limiting Form

Shibendu Mahata <sup>1</sup>, Norbert Herencsar <sup>2,\*</sup> and David Kubanek <sup>2</sup>

<sup>1</sup> Department of Electrical Engineering, Dr. B. C. Roy Engineering College, Durgapur 713206, West Bengal, India; shibendu.mahata@bcrec.ac.in

<sup>2</sup> Department of Telecommunications, Faculty of Electrical Engineering and Communication, Brno University of Technology, Technicka 12, 61600 Brno, Czech Republic; kubanek@vutbr.cz

\* Correspondence: herencsn@ieee.org; Tel.: +420-541-146-981

**Abstract:** This paper proposes a further generalization of the fractional-order filters whose limiting form is that of the second-order filter. This new filter class can also be regarded as a superset of the recently reported power-law filters. An optimal approach incorporating constraints that restricts the real part of the roots of the numerator and denominator polynomials of the proposed rational approximant to negative values is formulated. Consequently, stable inverse filter characteristics can also be achieved using the suggested method. Accuracy of the proposed low-pass, high-pass, band-pass, and band-stop filters for various combinations of design parameters is evaluated using the absolute relative magnitude/phase error metrics. Current feedback operational amplifier-based circuit simulations validate the efficacy of the four types of designed filters and their inverse functions. Experimental results for the frequency and time-domain performances of the proposed fractional-order band-pass filter and its inverse counterpart are also presented.

**Keywords:** analog filter approximation; current feedback operational amplifier; fractional-order filter; inverse filter; optimization; power-law filter; second-order filter



**Citation:** Mahata, S.; Herencsar, N.; Kubanek, D. Further Generalization and Approximation of Fractional-Order Filters and Their Inverse Functions of the Second-Order Limiting Form. *Fractal Fract.* **2022**, *6*, 209. <https://doi.org/10.3390/fractalfract6040209>

Academic Editor: Da-Yan Liu

Received: 10 February 2022

Accepted: 5 April 2022

Published: 8 April 2022

**Publisher's Note:** MDPI stays neutral with regard to jurisdictional claims in published maps and institutional affiliations.



**Copyright:** © 2022 by the authors. Licensee MDPI, Basel, Switzerland. This article is an open access article distributed under the terms and conditions of the Creative Commons Attribution (CC BY) license (<https://creativecommons.org/licenses/by/4.0/>).

## 1. Introduction

The concepts of fractional calculus [1], the branch of mathematics which generalizes the integration and differentiation operations, have seen widespread applications in various fields of science and engineering [2]. The Grunwald–Letnikov definition of a fractional derivative of order  $\alpha$  for a function  $f(t)$  is given by (1) [3].

$${}_a D_t^\alpha f(t) = \lim_{h \rightarrow 0} \frac{1}{h^\alpha} \sum_{j=0}^{\left[ \frac{t-a}{h} \right]} (-1)^j \binom{\alpha}{j} f(t-jh) \quad (1)$$

where  $[x]$  denotes the integer part of  $x$ ;  $\binom{\alpha}{j} = \frac{\Gamma(\alpha+1)}{\Gamma(j+1)\Gamma(\alpha-j+1)}$  represents the binomial coefficients;  $a$  and  $t$  are the bounds of the operation; and  $\alpha \in (0, 1)$ . Under zero initial conditions, the Laplace transformation of (1) is given by (2).

$$L\{{}_0 D_t^\alpha f(t)\} = s^\alpha F(s) \quad (2)$$

The presence of the additional tuning parameter  $\alpha$  provides several fundamental advantages to fractional-order (FO) filters when compared against the traditional (integer-order) filters: (i) exact meeting of design specifications, which implies precise control of filter roll-off characteristics. For instance, the fractional-order low-pass filter (FLPF) exhibits

a roll-off rate of  $-20(N + \alpha)$  decibel/decade (dB/dec), where  $N = 0, 1, \dots$ , and  $\alpha \in (0, 1)$ ; the same for the traditional filter is  $-20n$  dB/dec ( $n = 1, 2, \dots$ ) [3]. The roll-off rate of  $-20\alpha$  dB/dec, which finds application in the music industry [4], cannot be obtained using the integer-order filters. Similarly, a fractional-order band-pass filter (FBPF), in addition to exhibiting an asymmetric slope, can attain a roll-off extending down to 0 dB/dec [5]. In contrast, the minimum slope yielded for the classical band-pass filter, which always exhibits a symmetric magnitude-frequency behavior about the center frequency, is  $\pm 20$  dB/dec. Generalization of the traditional filters, such as the Butterworth [6], Chebyshev [7], shadow filter [8], etc., exploits the afore-mentioned advantages; (ii) various filter characteristics such as bandwidth, center frequency, quality factor, etc., are dependent on  $\alpha$  which provides an additional design parameter to the circuit designer, and, hence, better flexibility [9]; and (iii) FO filters (for example, the FO Sallen-Key filter [10]) may achieve improved stability range compared to their classical counterparts.

The FO filters can be modeled using the fractional-order transfer function (FTF), where the use of constant phase element for practical circuit implementation is required [11]. These constant phase elements, also known as the FO elements or fractance devices, provide an impedance phase characteristic which is independent of the frequency of operation and whose value is not limited to only  $+90$  or  $-90$  degrees, as is usual for classical inductors and capacitors [12]. Realization of FO filter circuits using the fractors can lead to reduced component count compared to the alternative technique involving the approximation of FO filters using the integer-order transfer function (ITF). For example, a 1.5<sup>th</sup>-order Butterworth filter can be realized using a single operational amplifier (op-amp), one FO capacitor, one conventional capacitor, and three resistors [13]. In contrast, a third-order approximant of the same filter for six decades of design bandwidth requires four current feedback op-amps (CFOAs), three traditional capacitors, and eight resistors [14]. Due to the absence of commercial fractance elements, the impedance characteristics of the FO capacitor can be emulated using passive RC ladder networks or active components [15]. For example, the Valsa network [16] emulates the FO capacitor behavior for three decades of frequency using a ladder structure comprising five resistors and five capacitors. Hence, the passive component count for the FTF-based FO filter circuit can also increase substantially.

Certain FO filters may be more conveniently modeled by determining their rational approximations. Two techniques exist in the literature for conversion of the FTF into its integer-order counterpart: (a) substitution of the rational approximation of the  $s^\alpha$  operator [17] in the FTF, as reported in [18], or further optimizing the obtained integer-order model to enhance the design bandwidth [14], and (b) direct determination of the ITF which approximates the magnitude and phase-frequency characteristics of the FO filter. For this purpose, either optimization techniques or curve-fitting procedures have been employed for the design of FO transitional filter [19], power-law filter (PLF) [20–23], etc.

The contributions of this paper are the following:

1. Further generalization of the FO filter of the second-order limiting form is proposed. It is demonstrated that the PLFs reported in [20–23] are also a small subset of the class of filters proposed in this work;
2. This new class of filters of the low-pass (LP), high-pass (HP), band-pass (BP), and band-stop (BS) type, which attains more generic magnitude and phase-frequency characteristics, is then approximated as a rational transfer function. The coefficients of the ITF models are optimally determined such that the poles and zeros of the approximant are restricted to reside in the left-half  $s$ -plane;
3. As reported in [21], the frequency-domain-based curve-fitting using the Sanathanan–Koerner least-squares method presented in [20,22,23] can lead to unstable inverse LP and inverse HP type PLFs for some design cases. The proposed approach to formulate the constraints, which is different from the method adopted in [21], helps convert the stable filter into its stable inverse counterpart also through a simple inversion. To the best of the authors' knowledge, these inverse filters, which further generalizes the models reported in [21], are also presented for the first time in the literature;

4. Circuit implementations for all the four filter types as well as their inverse counterparts are demonstrated on Simulation Program with Integrated Circuit Emphasis (SPICE) platform based on the CFOA being employed as an active component. Experimental measurements for the proposed FBPF and its corresponding inverse filter are also presented, which confirm their practical feasibility.

In the rest of the paper, the new theoretical filter transfer functions are introduced in Section 2 along with the proposed design technique. In Section 3, MATLAB simulations are conducted to investigate the performance of the proposed models; circuit simulations and experimental results are also presented in this section. Finally, the conclusions and future scope of research are outlined in Section 4.

## 2. Problem Formulation

### 2.1. Generalization of Power-Law Filter Transfer Function

The generalized FO filter transfer function whose characteristic polynomial depends on two FO capacitors of order  $\alpha$ , is given by (3) [24].

$$H(s) = \frac{cs^{2\alpha} + ds^\alpha + h}{s^{2\alpha} + 2as^\alpha + b} \quad (3)$$

where  $a, b, c, d$ , and  $h$  are constant coefficients.  $H(s)$  is always stable provided the conditions  $a^2 \geq b$ ,  $a < 0$ , or  $b < 0$  are avoided. Fractional step magnitude and phase behaviors of the LP, HP, BP, and BS types may be obtained from (3) by setting  $c = d = 0$ ,  $d = h = 0$ ,  $c = h = 0$ , and  $d = 0$ , respectively. An optimal approximant for the transfer function of the form  $h/(s^{2\alpha} + 2as^\alpha + b)$  was obtained using a multi-objective optimization routine [25]. In [26], three different transfer functions, such as  $h/(s^{1+\alpha} + as^\alpha + b)$ ,  $h/(s^{1+\alpha} + as + b)$ , and  $h/(s^{1+\alpha} + as^{0.5(1+\alpha)} + b)$ , were formulated and their coefficients were optimally determined to approximate the frequency-domain characteristics of the second-order LP filter  $1/(s^2 + s/Q + 1)$ , where the quality factor  $Q$  can be adjusted to any arbitrary value. Optimal rational approximations for FO filters of the LP, HP, and BP types, such as  $h/R(s)$ ,  $hs^{\alpha+\beta}/R(s)$ , and  $hs^\beta/R(s)$ , respectively, where  $R(s) = s^{\alpha+\beta} + as^\beta + b$ , and  $\beta \in (0, 1)$ , were also reported [27].

A new class of FO filter, as given by (4), can be proposed by introducing a FO exponent  $\beta$  in the filter transfer function defined in (3):

$$H_D^{\alpha,\beta}(s) = \left( \frac{cs^{2\alpha} + ds^\alpha + h}{s^{2\alpha} + 2as^\alpha + b} \right)^\beta \quad (4)$$

where  $\beta \in (0, 1]$  and  $\beta \in [-1, 0)$  leads to the standard and inverse filter characteristics, respectively. The transfer function, magnitude, and phase of the LP, HP, BP, and BS type proposed theoretical filters are presented in Table 1.

$H(s)$  is a special case of  $H_D^{\alpha,\beta}(s)$  when  $\beta = 1$ , which implies further generalization of the filter forms reported in [24]. The classical second-order filter can be obtained from (4) by choosing  $\alpha = \beta = 1$ . As a representative, Figure 1 shows the different magnitude and phase-frequency characteristic curves exhibited for the theoretical FLPF ( $c = 0$ ,  $d = 0$ ,  $h = 1$ ,  $a = 1$ ,  $b = 1$ ), with  $\alpha = 0.6$  and  $\beta = \{0.6, 0.8, 1\}$ . The introduction of the additional tuning parameter  $\beta$  in the proposed FO filter transfer function given by (4) can yield a much wider variety of magnitude and phase-frequency characteristics which is not possible to attain using only a single tuning knob  $\alpha$  in (3).

**Table 1.** Transfer function, magnitude, and phase of the proposed theoretical filters.

Filter Type	Transfer Function	Parameter	Expression
Low-pass	$\left(\frac{h}{s^{2\alpha} + 2as^\alpha + b}\right)^\beta$	Magnitude	$\frac{h^\beta}{[\omega^{4\alpha} + 4a^2\omega^{2\alpha} + b^2 + 2b\omega^{2\alpha} \cos(\alpha\pi) + 4ab\omega^\alpha \cos(\alpha\pi/2) + 4a\omega^{3\alpha} \cos(\alpha\pi/2)]^{\beta/2}}$
		Phase	$-\beta \tan^{-1} \left[ \frac{\omega^{2\alpha} \sin(\alpha\pi) + 2a\omega^\alpha \sin(\alpha\pi/2)}{\omega^{2\alpha} \cos(\alpha\pi) + 2a\omega^\alpha \cos(\alpha\pi/2) + b} \right]$
High-pass	$\left(\frac{cs^{2\alpha}}{s^{2\alpha} + 2as^\alpha + b}\right)^\beta$	Magnitude	$\frac{c^\beta \omega^{2\alpha\beta}}{[\omega^{4\alpha} + 4a^2\omega^{2\alpha} + b^2 + 2b\omega^{2\alpha} \cos(\alpha\pi) + 4ab\omega^\alpha \cos(\alpha\pi/2) + 4a\omega^{3\alpha} \cos(\alpha\pi/2)]^{\beta/2}}$
		Phase	$\beta \left( \alpha\pi - \tan^{-1} \left[ \frac{\omega^{2\alpha} \sin(\alpha\pi) + 2a\omega^\alpha \sin(\alpha\pi/2)}{\omega^{2\alpha} \cos(\alpha\pi) + 2a\omega^\alpha \cos(\alpha\pi/2) + b} \right] \right)$
Band-pass	$\left(\frac{ds^\alpha}{s^{2\alpha} + 2as^\alpha + b}\right)^\beta$	Magnitude	$\frac{d^\beta \omega^{\alpha\beta}}{[\omega^{4\alpha} + 4a^2\omega^{2\alpha} + b^2 + 2b\omega^{2\alpha} \cos(\alpha\pi) + 4ab\omega^\alpha \cos(\alpha\pi/2) + 4a\omega^{3\alpha} \cos(\alpha\pi/2)]^{\beta/2}}$
		Phase	$\beta \left( 0.5\alpha\pi - \tan^{-1} \left[ \frac{\omega^{2\alpha} \sin(\alpha\pi) + 2a\omega^\alpha \sin(\alpha\pi/2)}{\omega^{2\alpha} \cos(\alpha\pi) + 2a\omega^\alpha \cos(\alpha\pi/2) + b} \right] \right)$
Band-stop	$\left(\frac{cs^{2\alpha} + h}{s^{2\alpha} + 2as^\alpha + b}\right)^\beta$	Magnitude	$\left[ \frac{c^2\omega^{4\alpha} + h^2 + 2hc\omega^{2\alpha} \cos(\alpha\pi)}{\omega^{4\alpha} + 4a^2\omega^{2\alpha} + b^2 + 2b\omega^{2\alpha} \cos(\alpha\pi) + 4ab\omega^\alpha \cos(\alpha\pi/2) + 4a\omega^{3\alpha} \cos(\alpha\pi/2)} \right]^{\beta/2}$
		Phase	$\beta \left( \tan^{-1} \left[ \frac{c\omega^{2\alpha} \sin(\alpha\pi)}{c\omega^{2\alpha} \cos(\alpha\pi) + h} \right] - \tan^{-1} \left[ \frac{\omega^{2\alpha} \sin(\alpha\pi) + 2a\omega^\alpha \sin(\alpha\pi/2)}{\omega^{2\alpha} \cos(\alpha\pi) + 2a\omega^\alpha \cos(\alpha\pi/2) + b} \right] \right)$

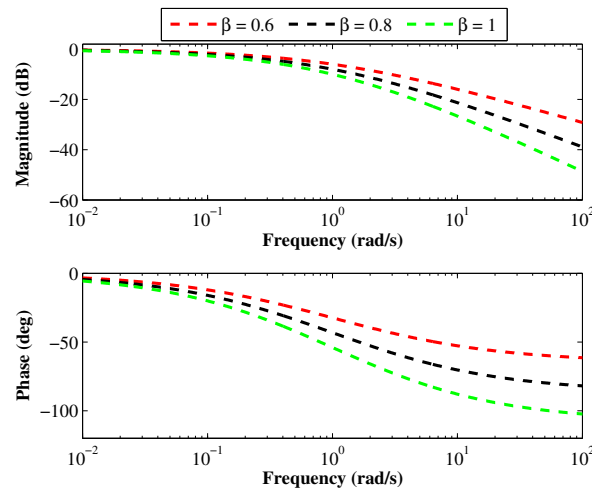


**Figure 1.** Magnitude and phase responses of the theoretical FLPF for different values of  $\beta$  with  $\alpha = 0.6$ .

A different form of double FO-exponent LP and HP filter transfer functions, such as  $\{1/(s^\alpha + 1)\}^\beta$  and  $\{s^\alpha/(s^\alpha + 1)\}^\beta$ , respectively, where  $\alpha, \beta \in (-2, 2)$ , were reported in [28]. Two FO elements-based band-stop filter of the form  $(s^p + k_1s^q + k_2)/(s^p + k_3s^q + k_2)$ , where,  $p = 1 + \beta_1 + \beta_2, q = 1 + \beta_2$ , and  $\beta_1, \beta_2 \in (0, 1)$ , was presented in [29], which is also unlike the proposed fractional-order band-stop filter (FBSF) model. Note that the transfer function of the PLF reported in [20–23] can be obtained from (4) by setting  $\alpha = 1$ . Therefore, the proposed FO filter transfer function also provides a further generalization of the PLF models. As an example, the magnitude and phase-characteristics of the theoretical LP type PLF [20–23] and that of the proposed filter, with  $(c = d = 0, h = a = b = 1, \beta = 0.7)$ , are compared in Figure 2. It can be seen that for the considered case (i.e.,  $\beta = 0.7$ ), the PLF attains only a single characteristic curve since  $\alpha$  is fixed at 1, whereas the proposed filter can achieve various other responses (viz.,  $\alpha = 0.6, 0.8$ ).

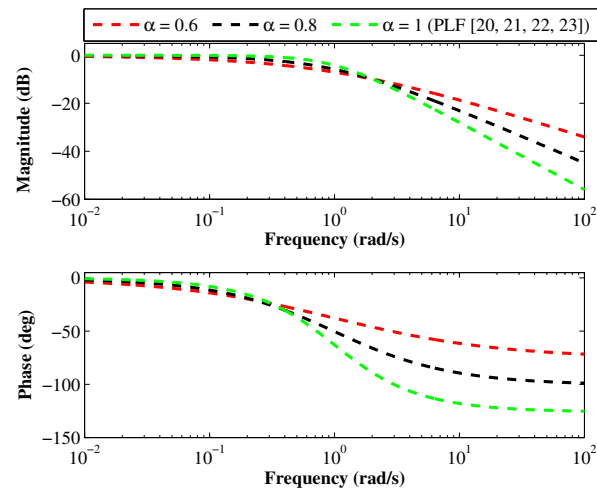


**Figure 2.** Magnitude and phase responses of the theoretical FLPF for different values of  $\alpha$  with  $\beta = 0.7$ .

2.2. Proposed Technique

Defining an ITF as per (5), where  $N$  is a positive integer, the frequency-domain characteristics of the theoretical FO filter may be approximated in the optimal sense by minimizing the mean absolute relative magnitude and phase errors between  $H_D^{\alpha,\beta}(j\omega)$  and  $H_P^{\alpha,\beta,N}(j\omega)$ .

$$H_P^{\alpha,\beta,N}(s) = \frac{A(s)}{B(s)} = \frac{\sum_{i=0}^N a_i s^i}{s^N + \sum_{k=0}^{N-1} b_k s^k} \tag{5}$$

For this purpose, the objective function for the proposed optimization (minimization) routine is formulated according to (6), subject to the nonlinear inequality constraints which ensure that the zeros and poles of  $H_P^{\alpha,\beta,N}(s)$  lie strictly on the left-half  $s$ -plane.

$$f = \frac{1}{L} \sum_{i=1}^L \left[ \left| 1 - \frac{|H_P^{\alpha,\beta,N}(j\omega_i, X)|}{|H_D^{\alpha,\beta}(j\omega_i)|} \right| + \left| 1 - \frac{\angle H_P^{\alpha,\beta,N}(j\omega_i, X)}{\angle H_D^{\alpha,\beta}(j\omega_i)} \right| \right] \tag{6}$$

Subject to:

- (i)  $a_k > 0$  ( $k = 0, 1, \dots, N$ );
- (ii)  $b_k > 0$  ( $k = 0, 1, \dots, N - 1$ );
- (iii) Real part of roots of  $A(s)$  and  $B(s) < 0$ .

where  $X$  denotes the vector of decision variables, i.e.,  $X = [a_N \ a_{N-1} \ \dots \ a_0 \ b_{N-1} \ b_{N-2} \ \dots \ b_0]$ ;  $L$  denotes the number of log-spaced sample points in the bandwidth  $[\omega_{\min}, \omega_{\max}]$  rad/s; and the dimension ( $D$ ) of the problem is  $2N + 1$ . The application of metaheuristics for the optimal approximation of FO filters and systems has shown promising performances [30]. The constrained composite differential evolution ( $C^2$ oDE) algorithm [31] can be employed as the optimization problem solver for this work.  $C^2$ oDE integrates the basic framework of composite differential evolution [32], with the constraint-handling mechanisms based on the feasibility rule [33] and the  $\epsilon$ -constrained method [34]. The detailed discussion of the  $C^2$ oDE algorithm can be found in [31]. The proposed objective function is minimized by  $C^2$ oDE, where the FO exponents  $\{\alpha, \beta\}$  of the theoretical filter transfer function, order of the proposed rational approximant ( $N$ ), length of data sample points ( $L$ ), lower limit ( $\omega_{\min}$ ), and upper limit ( $\omega_{\max}$ ) of the desired bandwidth are the user-defined inputs to the optimization routine. The metaheuristic search procedure of  $C^2$ oDE determines the

best feasible solution ( $X^*$ ), i.e., the vector of decision variables (coefficients of  $H_p^{\alpha,\beta,N}(s)$ ) which achieves the smallest value of  $f$  while also satisfying the design constraints, after  $maxrun$  number of independent trial runs of the algorithm are conducted. Therefore,  $X^*$  is declared as the near-global optimal solution at the end of the proposed search optimization procedure. In Figure 3, the flowchart of the proposed analog filter design technique is presented.

As highlighted in [35], the issue of design stability for the inverse filters is an important topic. A different set of constraints have been proposed here to ensure the approximant's stable and minimum phase response as compared to the Hurwitz determinant method employed in [21]. While forcing the coefficients  $a_k$  and  $b_k$  to be positive, the proposed constraints also ensure that the real part of all the roots of the numerator and denominator polynomials of  $H_p^{\alpha,\beta,N}(s)$  attains a negative value. Since all the zeros of the proposed approximant are constrained to lie in the left-half  $s$ -plane, inverting the transfer function  $H_p^{\alpha,\beta,N}(s)$ , i.e.,  $[H_p^{\alpha,\beta,N}(s)]^{-1}$ , provides the stable inverse filter characteristics for the proposed FLPF, fractional-order high-pass filter (FHPPF), FBPF, and FBSF. The inverse filter transfer functions proposed in this work are also different from those published in the literature [36–41]. Henceforth, the FO inverse LP, HP, BP, and BS filters will be abbreviated as FILPF, FIHPF, FIBPF, and FIBSF, respectively.

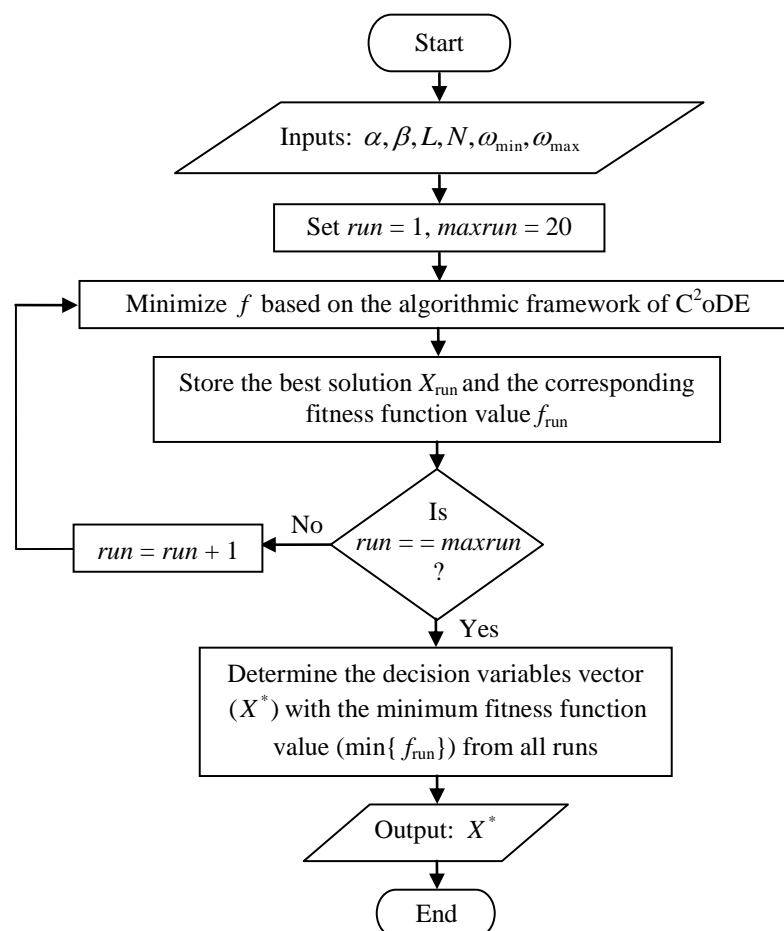


Figure 3. Flowchart of the proposed filter design technique.

### 3. Results and Discussions

In this work, the population size and the maximum number of function evaluations for  $C^2oDE$  are chosen as 100 and 10,000D, respectively; the remaining control parameters are set according to the recommendations provided in [31]. The lower bound of the decision

variables is chosen as  $10^{-6}$  while the upper bound is set as 20,000. For all the design cases presented in this paper,  $L = 100$ ,  $\omega_{\min} = 10^{-2}$  rad/s,  $\omega_{\max} = 10^2$  rad/s, and  $maxrun = 20$ , are chosen. The proposed optimization routine is implemented in MATLAB, where the roots of  $A(s)$  and  $B(s)$  for each search agent are determined using the roots() function. To evaluate the design accuracy, the absolute relative magnitude error (ARME) and the absolute relative phase error (ARPE) metrics are used. These error indices are defined as per (7) and (8), respectively:

$$ARME = \left| \frac{|H_D^{\alpha,\beta}(j\omega)| - |H_P^{\alpha,\beta,N}(j\omega)|}{|H_D^{\alpha,\beta}(j\omega)|} \right| \tag{7}$$

$$ARPE = \left| \frac{\angle H_D^{\alpha,\beta}(j\omega) - \angle H_P^{\alpha,\beta,N}(j\omega)}{\angle H_D^{\alpha,\beta}(j\omega)} \right| \tag{8}$$

### 3.1. Performance Analysis

#### 3.1.1. Fractional-Order Low-Pass Filter

The optimal model coefficients of the FLFPs ( $c = d = 0, h = a = b = 1$ ) for different combinations of  $\alpha, \beta$ , and  $N$  are presented in Table 2. The stability criteria are satisfied for all the design cases since the system poles are always located on the left-half  $s$ -plane. For instance, the poles of the proposed FLFP with  $N = 4$  and  $(\alpha, \beta) = (0.6, 0.8)$  are located at  $s = \{-0.0271, -0.2303, -1.2976, -9.5261\}$ . To achieve a stable FILPF, the zeros of the corresponding FLFP must reside on the left-half  $s$ -plane. It is noteworthy that the proposed design constraints in this regard are also satisfied. For example, the zeros of the afore-mentioned design case are located at  $s = \{-0.0315, -0.3949, -5.6393, -1054.7\}$ .

**Table 2.** Optimal coefficients of the proposed FLFPs for different values of  $\alpha, \beta$ , and  $N$ .

$\alpha$	$\beta$	$N$	$[a_N \ a_{N-1} \ \dots \ a_0]$	$[b_{N-1} b_{N-2} \ \dots \ b_0]$
0.6	0.6	3	0.0142 2.5299 6.6189 0.4942	11.4218 9.2670 0.5131
		4	0.0114 3.0287 25.5717 13.7481 0.4771	24.2389 55.7542 16.8974 0.4922
		5	0.0092 3.4666 61.4831 110.5999 22.6230 0.4607	41.6920 208.3549 178.6875 26.2131 0.4730
0.6	0.8	3	0.0013 0.9827 1.6323 0.0935	4.7579 2.3646 0.0980
		4	0.0010 1.0608 6.4002 2.5499 0.0741	11.0810 15.1524 3.2481 0.0770
		5	0.0008 1.1094 15.6780 21.3117 3.5163 0.0625	21.2276 62.7773 37.1129 4.2024 0.0646
0.7	0.6	3	0.0051 1.6591 4.5010 0.3897	7.7235 5.9418 0.3968
		4	0.0041 1.8637 16.5030 9.4477 0.3705	17.7793 34.5354 11.0523 0.3761
		5	0.0031 2.0251 38.1221 70.6279 15.5349 0.3518	32.3963 132.0535 107.9572 17.2623 0.3562
0.9	0.5	3	0.0021 1.4230 6.3582 0.9979	7.7812 7.7812 1.0000
		4	0.0018 1.5155 18.6555 16.4228 0.9982	17.9383 37.3110 17.9383 1.0000
		5	0.0014 1.5881 38.2769 97.7768 30.9821 0.9986	32.5702 136.0537 136.0537 32.5702 1.0000

The effect due to variations of  $N$  on the accuracy of the proposed FLFPs is presented in Table 3 by considering the maximum (max) and mean values of ARME and ARPE metrics. In total, 1000 log-spaced data sample points are considered for evaluating the mean error. This is due to the fact that the mean error remains nearly the same if a higher number of data points are used; while the error marginally increases if a lower number of sample points are chosen. For example, the values of {mean ARME (dB), mean ARPE (dB)} attained by the proposed FLFP with  $\alpha = 0.7, \beta = 0.6$ , and  $N = 4$  for 100, 1000, and 10,000 sample points are  $\{-36.36, -32.69\}, \{-36.53, -32.82\}$ , and  $\{-36.54, -32.83\}$ , respectively. Similar results are also obtained for the other design cases, which justify the selection of 1000 sample points for the evaluation of the mean errors. It is also found that the accuracy increases (i.e., error reduces) with an increase in the design order ( $N$ ) for all the cases. For instance, considering

the FLPF for  $(\alpha, \beta) = (0.9, 0.5)$ , the max and mean values of ARME for  $N = \{3, 4, 5\}$  are  $\{-20.25, -25.36, -31.21\}$  dB and  $\{-35.53, -43.34, -51.13\}$  dB, respectively; similarly, the max and mean ARPE values are  $\{-20.13, -25.31, -31.51\}$  dB and  $\{-31.91, -39.78, -47.24\}$  dB, respectively. These results are in accordance with the fact that the accuracy of approximating any FTF with an integer-order one improves as  $N$  increases; the modeling error being theoretically zero when the integer-order model has an order of infinity. Since such infinite-dimensional systems are impractical, a trade-off between accuracy and order (design/hardware complexity) is a pertinent issue in the rational approximation of any FO system.

**Table 3.** Performance indices of the designed FLPFs for different values of  $N$ .

$\alpha$	$\beta$	$N$	ARME (dB)		ARPE (dB)		$M_C$ (dB)	$\theta_C$ (deg)	$\omega_M$ (rad/s)	$\omega_\theta$ (rad/s)
			Max	Mean	Max	Mean				
0.6	0.6	3	-15.00	-26.51	-13.04	-21.96	-5.937	-35.72	1.0210	0.7918
		4	-19.00	-34.16	-18.72	-29.74	-6.054	-30.85	0.9886	1.1610
		5	-24.33	-41.81	-26.29	-37.09	-6.013	-32.99	1.0030	0.9484
0.6	0.8	3	-17.93	-28.88	-15.09	-25.73	-8.348	-45.08	0.9380	0.8406
		4	-23.49	-36.76	-21.59	-33.59	-7.887	-42.35	1.0380	1.0530
		5	-29.09	-44.52	-29.88	-41.41	-8.092	-43.52	0.9867	0.9768
0.7	0.6	3	-15.98	-28.08	-14.46	-24.99	-5.539	-40.24	1.0060	0.8658
		4	-20.75	-36.53	-19.84	-32.82	-5.569	-36.66	0.9995	1.0820
		5	-26.28	-44.21	-26.75	-40.12	-5.564	-38.24	0.9999	0.9723
0.9	0.5	3	-20.25	-35.53	-20.13	-31.91	-3.555	-41.18	1.0220	0.9725
		4	-25.36	-43.34	-25.31	-39.78	-3.685	-40.19	0.9895	1.0150
		5	-31.21	-51.13	-31.51	-47.24	-3.628	-40.63	1.0040	0.9949

The magnitude ( $M_{CT}$ ) of the theoretical FLPF at the frequency of 1 rad/s for  $(\alpha, \beta) = (0.6, 0.6)$ ,  $(0.6, 0.8)$ ,  $(0.7, 0.6)$ , and  $(0.9, 0.5)$  is  $-6.023$  dB,  $-8.031$  dB,  $-5.565$  dB, and  $-3.643$  dB, respectively. The phase ( $\theta_{CT}$ ) of the theoretical filters at 1 rad/s for the same combinations of  $(\alpha, \beta)$  is  $-32.40^\circ$ ,  $-43.21^\circ$ ,  $-37.81^\circ$ , and  $-40.51^\circ$ , respectively. The magnitude and phase of the proposed filters at 1 rad/s, denoted by  $M_C$  and  $\theta_C$ , respectively, are presented in Table 3. Results reveal that both these values approach the theoretical ones for all the design cases as  $N$  is increased. The frequency values attained by the proposed FLPF at  $M_{CT}$  and  $\theta_{CT}$  are denoted by  $\omega_M$  and  $\omega_\theta$ , respectively. As demonstrated in Table 3, these performance indices also approach the theoretical frequency value of 1 rad/s with an increase in  $N$ .

Figure 4a highlights the improved accuracy in the magnitude and phase responses of the optimal FLPFs for the design case  $(\alpha = 0.7, \beta = 0.6)$  when  $N$  is increased from 3 to 5. Further confirmation is provided in Figure 4b, which shows the reduction in ARME and ARPE with an increase in  $N$ .

The magnitude responses of the proposed FLPFs ( $N = 4$ ) for  $(\alpha, \beta) = (0.6, 0.8)$  and  $(0.9, 0.5)$  and their corresponding inverse counterparts, i.e., FILPFs ( $N = 4$ ) for  $(\alpha, \beta) = (0.6, -0.8)$  and  $(0.9, -0.5)$ , are presented in Figure 5a, and the phase responses are shown in Figure 5b. Both the design cases exhibit proximity with the theoretical responses in the desired bandwidth. The zeros and poles of the FLPF for  $(\alpha, \beta) = (0.9, 0.5)$  are located at  $\{-0.0657, -0.8830, -11.5331, -829.4627\}$ , and  $\{-0.0640, -0.6091, -1.6418, -15.6234\}$ , respectively, in the  $s$ -plane, which implies that both the FLPF and its inverse counterpart are stable.

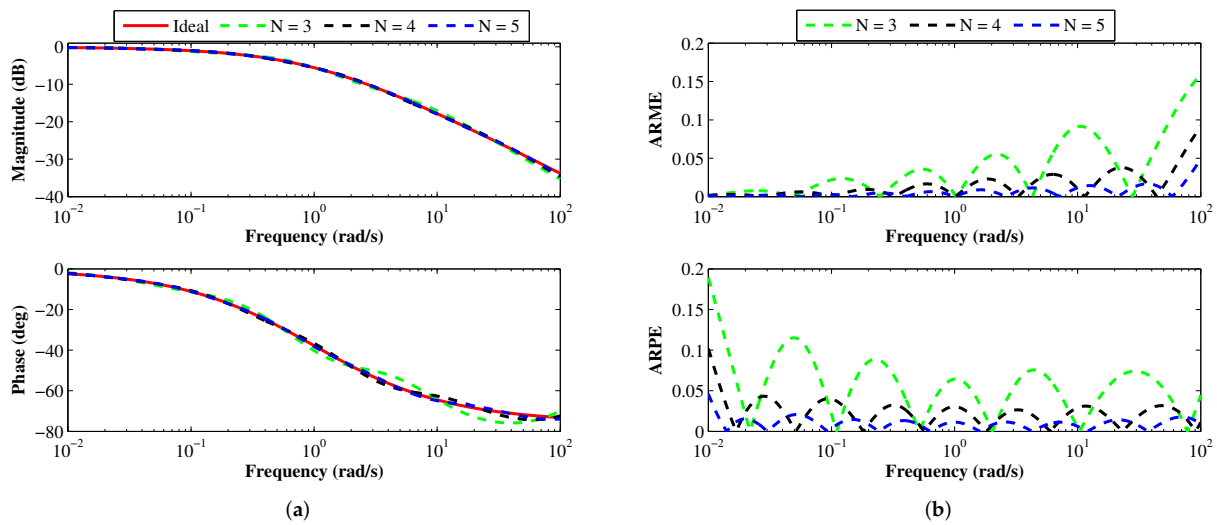


Figure 4. (a) Magnitude, phase and (b) ARME, ARPE responses of the proposed FLPF ( $\alpha = 0.7$ ,  $\beta = 0.6$ ) for different values of  $N$ .

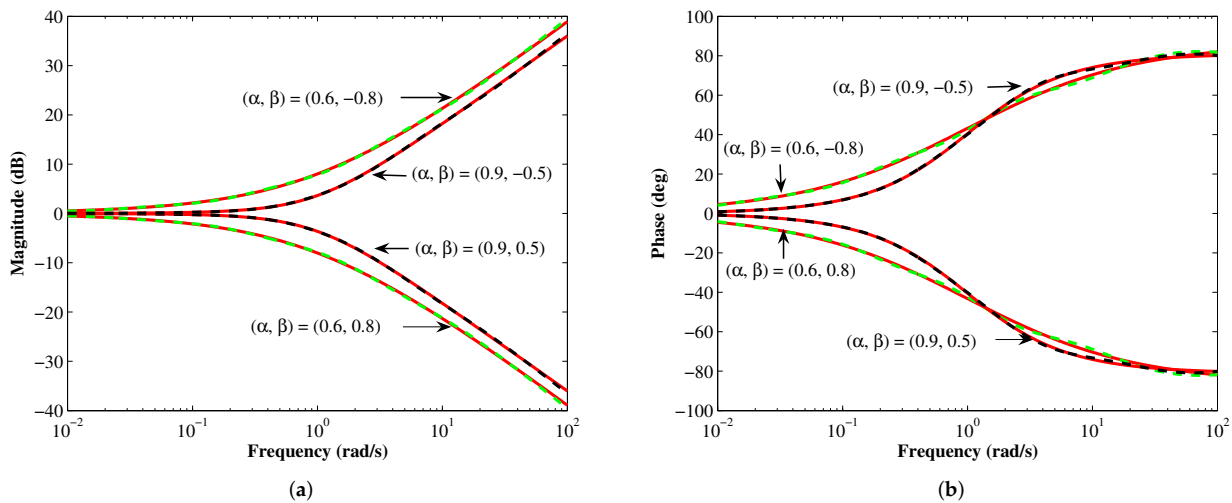


Figure 5. (a) Magnitude and (b) phase responses of the proposed FLPFs and FILPFs for  $N = 4$ . The theoretical response is shown in solid red.

### 3.1.2. Fractional-Order High-Pass Filter

The well-known LP-to-HP transformation technique [42], which involves replacing  $s$  with  $1/s$  in the FLPF transfer function, can convert the FLPF models presented in Table 2 into the FHPFs of the same order. The proposed technique can also allow the optimal design of FHPFs directly without obtaining the FLPF model in the first stage. In Table 4, the stable FHPF approximants for  $(\alpha, \beta) = (0.8, 0.5)$  and  $(0.7, 0.7)$  with  $(d = h = 0, c = a = b = 1)$  are obtained by carrying out the proposed optimization technique for different values of  $N$ . For instance, the poles and zeros of the FHPF with  $(\alpha, \beta, N) = (0.8, 0.5, 4)$  are obtained as  $\{-0.0530, -0.4949, -2.0205, -18.8688\}$  and  $\{-0.0025, -0.0972, -1.2887, -17.8685\}$ , respectively, in the  $s$ -plane. Such pole-zero locations justify that both the FHPF and its inverse model are stable.

The max and mean indices of the ARME and ARPE metrics are evaluated for the proposed FHPF transfer functions, as shown in Table 5. A similar finding regarding the improvement in accuracy with an increase in the design order is also noted here. The  $\{M_{CT}, \theta_{CT}\}$  values of the theoretical FHPF for  $(\alpha, \beta) = (0.8, 0.5)$  are  $\{-4.178 \text{ dB}, 35.99^\circ\}$ ; for  $(\alpha, \beta) = (0.7, 0.7)$ , these are  $\{-6.488 \text{ dB}, 44.09^\circ\}$ . The  $M_C, \theta_C, \omega_M,$  and  $\omega_\theta$  parameters attained

by the designed approximants for these cases are shown in Table 5, which highlights an improved proximity with the theoretical values for an increasing  $N$ .

Figure 6a,b present the magnitude and phase plots, respectively, of both the optimal FHPFs and their inverse functions, for  $N = 4$ . The frequency-domain characteristics of the approximants closely match with those of the theoretical responses.

**Table 4.** Optimal coefficients of the proposed FHPFs for different values of  $\alpha, \beta$ , and  $N$ .

$\alpha$	$\beta$	$N$	$[a_N a_{N-1} \dots a_0]$	$[b_{N-1} b_{N-2} \dots b_0]$
0.8	0.5	3	0.9932 7.8453 2.0344 0.0068	9.8797 9.8797 1.0000
		4	0.9944 19.1491 24.7984 2.2881 0.0056	21.4372 49.5967 21.4372 1.0000
		5	0.9956 35.4326 126.2330 54.3189 2.5130 0.0044	37.9456 180.5519 180.5519 37.9456 1.0000
0.7	0.7	3	0.9806 14.6603 8.9401 0.0051	19.1412 35.6366 9.0971
		4	0.9838 29.7348 70.3640 12.4674 0.0062	34.9174 142.9660 108.5833 12.1205
		5	0.9867 49.5131 277.8629 204.4321 15.4272 0.0055	55.3552 426.0090 692.3231 257.6597 14.6294

**Table 5.** Performance indices of the designed FHPFs for different values of  $N$ .

$\alpha$	$\beta$	$N$	ARME (dB)		ARPE (dB)		$M_C$ (dB)	$\theta_C$ (deg)	$\omega_M$ (rad/s)	$\omega_\theta$ (rad/s)
			Max	Mean	Max	Mean				
0.8	0.5	3	-16.36	-30.39	-15.52	-26.32	-4.016	37.42	0.9607	1.0750
		4	-20.88	-38.15	-20.54	-34.09	-4.253	35.31	1.0240	0.9563
		5	-26.75	-45.88	-27.31	-41.43	-4.150	36.25	0.9931	1.0150
0.7	0.7	3	-21.94	-32.77	-16.23	-28.43	-6.697	45.32	1.0450	1.0890
		4	-27.92	-40.83	-21.92	-36.56	-6.394	43.54	0.9772	0.9723
		5	-33.70	-48.61	-29.96	-44.31	-6.527	44.29	1.0100	1.0130

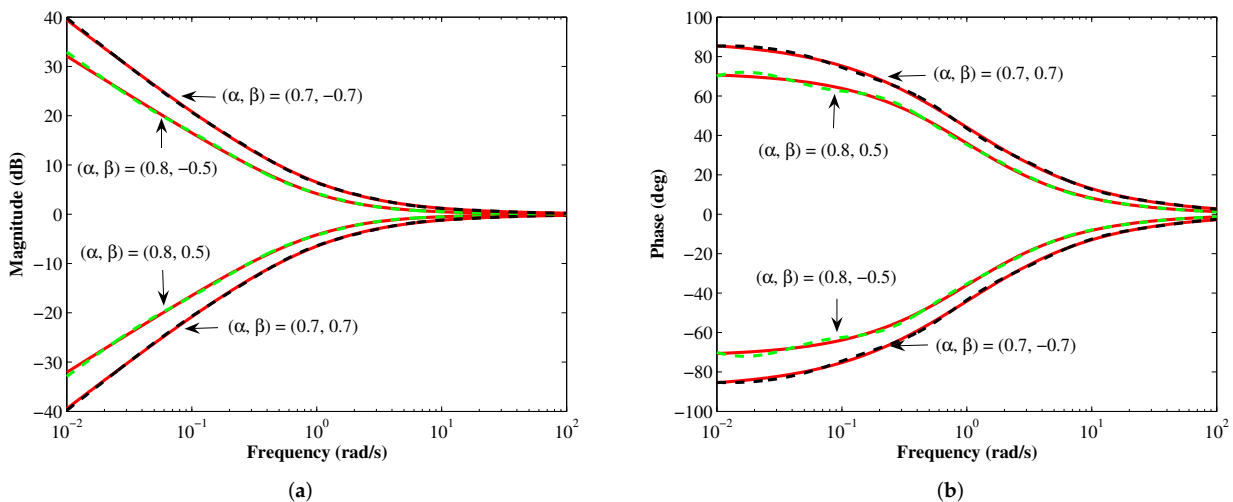


**Figure 6.** (a) Magnitude and (b) phase responses of the proposed FHPFs and FIHPFs for  $N = 4$ . The theoretical response is shown in solid red.

### 3.1.3. Fractional-Order Band-Pass Filter

The optimal coefficients of the FBPFs for two different cases, such as  $(\alpha, \beta) = (0.65, 0.85)$  and  $(0.7, 0.4)$ , with  $(c = h = 0, d = a = b = 1)$ , and  $N$  varying from 3 to 7, are presented in Table 6. For  $(\alpha, \beta, N) = (0.65, 0.85, 4)$ , the zeros and poles are located at  $\{-0.0052, -0.0913, -10.9496, -191.2333\}$  and  $\{-0.0261, -0.2131, -4.6931, -38.2753\}$ , respectively, in the  $s$ -plane. Hence, the proposed model can also be inverted to yield a stable FIBPF. A similar comment can also be made about all the other design orders and cases presented in Table 6.

However, cancellation of a pair of pole-zero occurs for odd values of  $N$  of the designed FBPFs. For example, the zeros and poles of the FBPF for  $(\alpha, \beta, N) = (0.65, 0.85, 5)$  are located at  $s = \{-0.0048, -0.0792, -1.0000, -12.6216, -210.4950\}$  and  $s = \{-0.0233, -0.1947, -1.0000, -5.1365, -42.8770\}$ , respectively. Therefore, cancellation of the pole-zero pair occurring at  $s = -1$  converts the fifth-order FBPF into a fourth-order one. Hence, it may be inferred that the design of FBPFs for even values of  $N$  is only appropriate. This issue of order truncation is also reflected in the modeling performance, as shown in Table 7, where the ARME and ARPE values for  $N = 5$  and  $7$  are close to those obtained for  $N = 4$  and  $6$ , respectively. However, a large improvement in accuracy is exhibited between two even values of  $N$ .

**Table 6.** Optimal coefficients of the proposed FBPFs for different values of  $\alpha, \beta$ , and  $N$ .

$\alpha$	$\beta$	$N$	$[a_N \ a_{N-1} \ \dots \ a_0]$	$[b_{N-1} \ b_{N-2} \ \dots \ b_0]$
0.65	0.85	3	0.0455 4.3916 4.3916 0.0455	14.0152 14.0152 1.0000
		4	0.0340 6.8775 71.8572 6.8775 0.0340	43.2076 189.9142 43.2076 1.0000
		5	0.0324 7.2641 93.9189 93.9189 7.2641 0.0324	49.2315 278.9397 278.9397 49.2315 1.0000
		6	0.0250 9.5746 317.2759 1481.1000 317.2759 9.5746 0.0250	95.0273 1388.1000 3966.1000 1388.1000 95.0273 1.0000
		7	0.0242 9.9057 365.7414 2150.5001 2150.5001 365.7414 9.9057 0.0242	102.9711 1704.5000 6397.6000 6397.6000 1704.5000 102.9711 1.0000
		3	0.2225 12.8293 12.8293 0.2225	22.5980 22.5980 1.0000
		4	0.1890 24.6291 220.2190 24.6291 0.1890	62.3458 342.9724 62.3458 1.0000
0.7	0.4	5	0.1853 26.4413 291.1292 291.1292 26.4413 0.1853	69.4012 483.2816 483.2816 69.4012 1.0000
		6	0.1622 40.1465 1131.1000 4864.2000 1131.1000 40.1465 0.1622	128.0391 2342.3000 7601.1000 2342.3000 128.0391 1.0000
		7	0.1595 42.2490 1326.8000 7221.5000 7221.5000 1326.8000 42.2490 0.1595	137.9077 2840.7000 11974.0000 11974.0000 2840.7000 137.9077 1.0000

The  $M_{CT}$  values of the theoretical FBPF for  $(\alpha, \beta) = (0.65, 0.85)$  and  $(\alpha, \beta) = (0.7, 0.4)$  are  $-8.221$  dB and  $-3.710$  dB, respectively, whereas,  $\theta_{CT} = 0^\circ$  for both the cases. The bandwidth (BW) of the theoretical filter, which represents the difference between the upper and lower half-power frequencies, is  $5.858$  rad/s and  $12.289$  rad/s for  $(\alpha, \beta) = (0.65, 0.85)$  and  $(0.7, 0.4)$ , respectively. The  $M_C, \theta_C$ , and BW yielded by the proposed approximants for various values of  $N$  are presented in Table 7. It is found that (i)  $\theta_C$  for all the cases is close to the theoretical value; (ii) the error index  $\delta_M = |M_{CT} - M_C|$  reduces as  $N$  (considering the even values) is increased. For example,  $\delta_M$  attained by the proposed FBPF with  $(\alpha, \beta) = (0.7, 0.4)$  are  $0.712$  dB and  $0.014$  dB for  $N = 4$  and  $N = 6$ , respectively; and (iii) the difference in the bandwidth between the theoretical and proposed models also reduces with an increased design order. For instance, the BW yielded by the proposed FBPF for the case  $(\alpha, \beta) = (0.65, 0.85)$  with  $N = 4$  is  $6.073$  rad/s, whereas the same for  $N = 6$  is obtained as  $5.835$  rad/s. These findings indicate an improved accuracy for the sixth-order approximant with respect to the theoretical anticipation (BW =  $5.858$  rad/s).

Figure 7a,b show the magnitude and phase plots of the proposed fourth-order FBPFs and their corresponding inverse transfer functions. Good agreement with the theoretical responses is obtained for both the test cases.

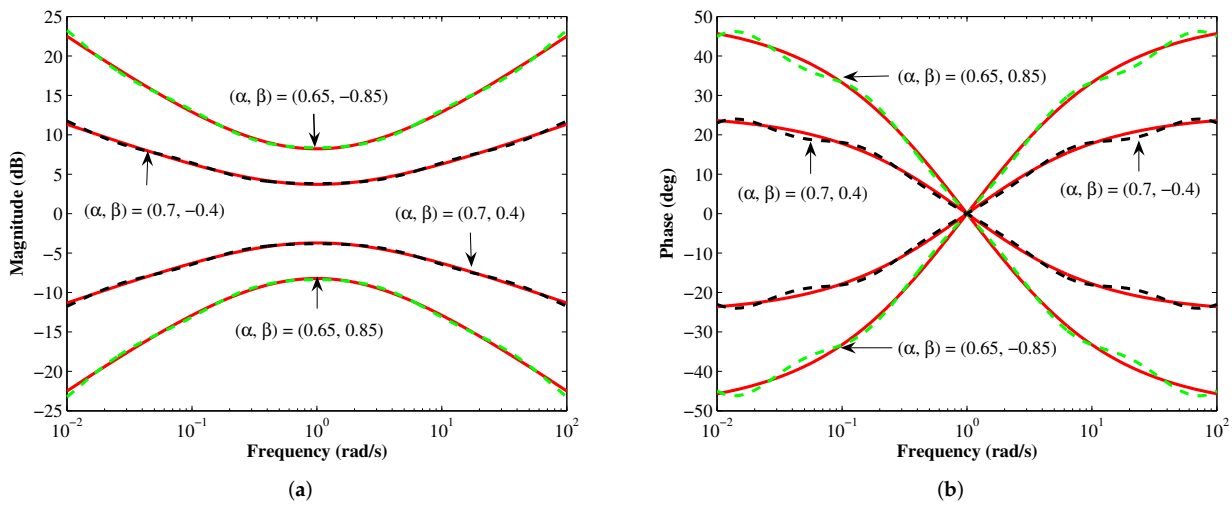


**Figure 7.** (a) Magnitude and (b) phase responses of the proposed FBPFs and FIBPFs for  $N = 4$ . The theoretical response is shown in solid red.

**Table 7.** Performance indices of the designed FBPFs for different values of  $N$ .

$\alpha$	$\beta$	$N$	ARME (dB)		ARPE (dB)		BW (rad/s)	$M_C$ (dB)	$\theta_C$ (deg)
			Max	Mean	Max	Mean			
0.65	0.85	3	-14.76	-19.32	-4.86	-11.75	13.205	-9.527	-0.0035
		4	-21.68	-34.50	-17.52	-27.36	6.073	-8.358	-0.0070
		5	-23.21	-34.64	-15.06	-25.71	6.417	-8.433	-0.0067
		6	-36.08	-49.89	-30.04	-41.07	5.835	-8.242	-0.0079
		7	-38.61	-49.95	-27.18	-39.68	5.840	-8.255	-0.0078
0.7	0.4	3	-18.03	-22.91	-3.53	-9.83	25.571	-4.676	-0.0015
		4	-26.72	-38.04	-15.16	-24.90	11.947	-3.812	-0.0037
		5	-28.00	-37.99	-12.91	-23.35	12.380	-3.868	-0.0035
		6	-41.30	-53.22	-27.44	-38.60	12.601	-3.724	-0.0043
		7	-43.93	-53.12	-24.66	-37.14	12.621	-3.734	-0.0042

### 3.1.4. Fractional-Order Band-Stop Filter

Table 8 presents the optimal values of coefficients of the FBSF approximants ( $d = 0, c = h = a = b = 1$ ) obtained for  $N = \{4, 6\}$  with two different values of  $(\alpha, \beta)$ , such as  $(0.75, 0.65)$  and  $(0.6, 0.9)$ . Stability and minimum phase response are attained for all the designed models. For example, the locations of the zeros and poles of the proposed FBSF for  $(\alpha, \beta, N) = (0.75, 0.65, 4)$  in the  $s$ -plane are at  $\{-0.0486, -0.7257+0.6880i, -0.7257-0.6880i, -20.5874\}$  and  $\{-0.0444, -0.3934, -2.5419, -22.5195\}$ , respectively. Similar to the FBPFs, a pole-zero pair occurs at  $s = -1$  for odd values of  $N$ , which can lead to order truncation. Hence, designs for only even values of  $N$  are presented here. The improvement in modeling accuracy with increasing  $N$  is justified using the max and mean values of ARME and ARPE, as presented in Table 9.

The theoretical FBSF yields the  $\{M_{CT}, BW\}$  of  $\{-7.252 \text{ dB}, 1.754 \text{ rad/s}\}$  and  $\{-7.768 \text{ dB}, 3.329 \text{ rad/s}\}$  for  $(\alpha, \beta) = (0.75, 0.65)$  and  $(0.6, 0.9)$ , respectively;  $\theta_{CT} = 0^\circ$  for both the design cases. The values of  $M_C, \theta_C$ , and BW attained by the optimal models are presented in Table 9, which confirms good agreement with the theory.

The magnitude and phase plots of the fourth-order FBSFs and FIBSFs are illustrated in Figure 8a,b, respectively. The responses of the proposed approximants remain in proximity with the theoretical characteristics throughout the design bandwidth.

**Table 8.** Optimal coefficients of the proposed FBSFs for different values of  $\alpha, \beta$ , and  $N$ .

$\alpha$	$\beta$	$N$	$[a_N a_{N-1} \dots a_0]$				$[b_{N-1} b_{N-2} \dots b_0]$				
0.75	0.65	4	0.9888	21.8400	31.5924	21.8400	0.9888	25.4992	68.2322	25.4992	1.0000
		6	0.9926	58.0809	430.8486	556.5188	430.8486	58.0809	0.9926	62.5308	575.3021
0.6	0.9	4	0.9562	31.9360	76.3241	31.9360	0.9562	41.7298	179.7455	41.7298	1.0000
		6	0.9683	77.7410	845.4961	1556.4000	845.4961	77.7410	0.9683	90.9584	1287.8000

**Table 9.** Performance indices of the designed FBSFs for different values of  $N$ .

$\alpha$	$\beta$	$N$	ARME (dB)		ARPE (dB)		BW (rad/s)	$M_C$ (dB)	$\theta_C$ (deg)
			Max	Mean	Max	Mean			
0.75	0.65	4	-30.30	-43.99	-15.30	-28.03	2.018	-6.991	0.0186
		6	-43.71	-57.38	-25.92	-41.60	1.793	-7.196	0.0213
0.6	0.9	4	-32.43	-41.32	-15.42	-26.59	3.709	-7.563	0.0102
		6	-48.63	-56.24	-28.33	-41.33	3.350	-7.736	0.0119

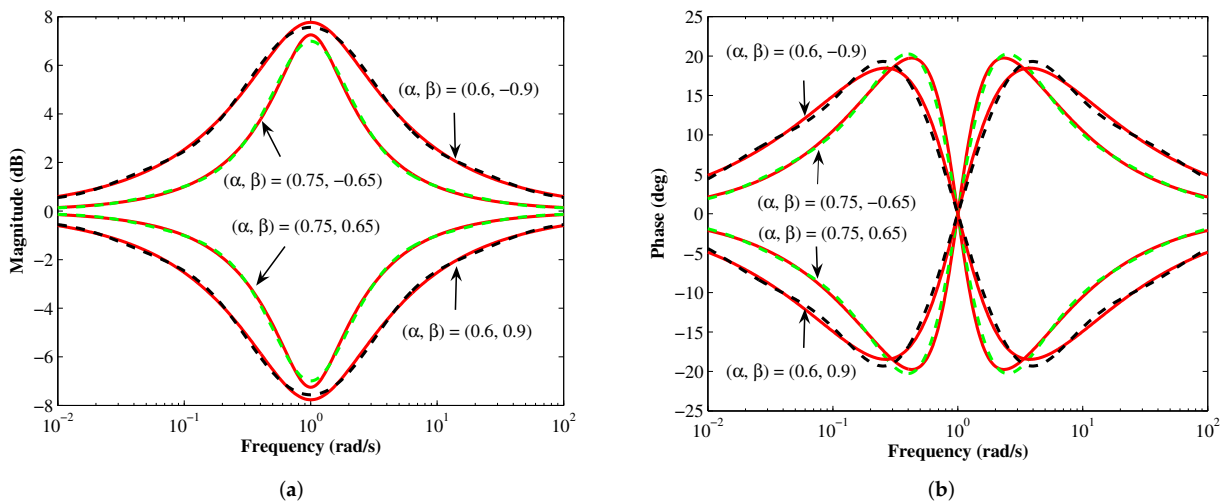


**Figure 8.** (a) Magnitude and (b) phase responses of the proposed FBSFs and FIBSFs for  $N = 4$ . The theoretical response is shown in solid red.

### 3.1.5. Comparison with the Literature

Comparisons regarding the modeling accuracy for the designed filters with the PLFs reported in the literature [20] are carried out. For demonstration purposes, the value of  $\beta$  is fixed as 0.3, whereas, two different values of  $\alpha$  (viz., 0.7 and 1), are considered for each type of filter. The designs reported in the published literature can model (4) for only  $\alpha = 1$ . Hence, such a method is not applicable for the design of generalized PLFs (where fractional value of  $\alpha$  such as 0.7 occurs); in contrast, the proposed method exhibits no such limitation. For comparison purposes, the values of quality factor and pole frequency for the PLFs reported in [20] are chosen as 0.5 and 1 rad/s, respectively. Therefore, the coefficients of the theoretical PLF transfer function in [20] are the same as that of the values of the filter coefficients  $a, b, c, d$ , and  $h$  chosen in Sections 3.1.1–3.1.4. The coefficients of the FLPF, FHPF, FBPF, and FBSF approximants based on the proposed method and the cited literature are presented in Table 10. Results presented in Table 11 show that the proposed filters attain comparable or lower ARME and ARPE values than the designs published in the literature for  $\alpha = 1$ .

**Table 10.** Coefficients of the proposed and reported filters for  $\beta = 0.3$  (NA: Not Applicable).

Type	Reference	$\alpha$	$[a_N a_{N-1} \dots a_0]$	$[b_{N-1} b_{N-2} \dots b_0]$
FLPF	[20]	0.7	NA	NA
	Present Work	0.7	0.0848 11.9870 109.7033 87.4632 4.6137	43.3927 178.5692 96.6050 4.6538
	[20]	1	0.02219 6.6070 171.1000 877.9000 999.4000	58.4100 578.6000 1477.0000 999.5000
	Present Work	1	0.0197 7.1837 219.3990 1221.6000 1427.9000	70.6331 781.3135 2078.2000 1427.9000
FHFPF	[20]	0.7	NA	NA
	Present Work	0.7	0.9914 18.7939 23.5728 2.5757 0.0182	20.7582 38.3705 9.3241 0.2149
	[20]	1	1.0000 0.8784 0.1712 0.006611 $2.22 \times 10^{-5}$	1.4780 0.5789 0.05844 0.001001
	Present Work	1	1.0000 0.8556 0.1537 0.0050 $1.379 \times 10^{-5}$	$1.4555 0.5472 0.0495 7.0034 \times 10^{-4}$
FBPF	[20]	0.7	NA	NA
	Present Work	0.7	0.2927 32.2869 264.4314 32.2869 0.2927	64.3533 368.5848 64.3533 1.0000
	[20]	1	0.2457 18.1300 97.4600 18.1300 0.2457	31.8200 99.4300 31.8200 1.0000
	Present Work	1	0.1772 19.9502 149.8006 19.9502 0.1772	48.3274 189.2569 48.3274 1.0000
FBSF	[20]	0.7	NA	NA
	Present Work	0.7	0.9919 23.9259 47.8177 23.9259 0.9919	25.9647 66.3058 25.9647 1.0000
	[20]	1	0.9994 0.9467 2.0690 0.9467 0.9994	1.5350 2.2660 1.5350 1.0000
	Present Work	1	0.9993 0.9207 2.0600 0.9207 0.9993	1.5080 2.2460 1.5080 1.0000

**Table 11.** Error metrics comparison of the proposed filters with the reported literature for  $\beta = 0.3$  (NA: Not Applicable).

Type	Reference	$\alpha$	ARME (dB)		ARPE (dB)	
			Max	Mean	Max	Mean
FLPF	[20]	0.7	NA	NA	NA	NA
	Present Work	0.7	-21.59	-38.13	-16.17	-28.87
	[20]	1	-23.82	-50.60	-33.80	-51.11
	Present Work	1	-29.17	-53.97	-35.52	-52.44
FHFPF	[20]	0.7	NA	NA	NA	NA
	Present Work	0.7	-21.55	-38.12	-16.18	-28.87
	[20]	1	-23.78	-50.68	-33.66	-51.78
	Present Work	1	-27.73	-52.98	-35.18	-52.54
FBPF	[20]	0.7	NA	NA	NA	NA
	Present Work	0.7	-28.15	-40.40	-15.21	-25.08
	[20]	1	-11.50	-13.19	-11.69	-26.76
	Present Work	1	-23.87	-35.13	-15.42	-25.35
FBSF	[20]	0.7	NA	NA	NA	NA
	Present Work	0.7	-39.47	-50.71	-15.61	-27.11
	[20]	1	-9.56	-49.46	-1.41	-33.64
	Present Work	1	-11.63	-48.97	-1.64	-33.12

### 3.2. Circuit Realization

#### 3.2.1. SPICE Validation

Practical implementations of FO filters using integrated forms [18,22], discrete components [5,13], and field-programmable analog arrays [23,43] have been reported. The use of CFOAs for electronic filter realization has gained prominence due to several reasons, such as improved gain-bandwidth product, lower component count, etc. [44]. Previous works on the applicability of CFOAs for FO filter implementation can be found in [21,39]. The CFOA-based circuit topology reported in [21] can be used to realize the proposed filters and

their inverse counterparts. The circuit (see Figure 9) and its transfer function are repeated here for the sake of completeness.

$$\frac{V_{OUT}(s)}{V_{IN}(s)} = \frac{R_{out}}{R_{in}} \times \frac{\frac{R}{R_1} s^N + \sum_{i=1}^N \frac{s^{N-i}}{R_1 R^{i-1} \prod_{k=1}^i \frac{R_{k+1}}{R_k} C_k}}{s^N + \sum_{i=1}^N \frac{s^{N-i}}{R_F R^{i-1} \prod_{k=1}^i C_k}} \quad (9)$$

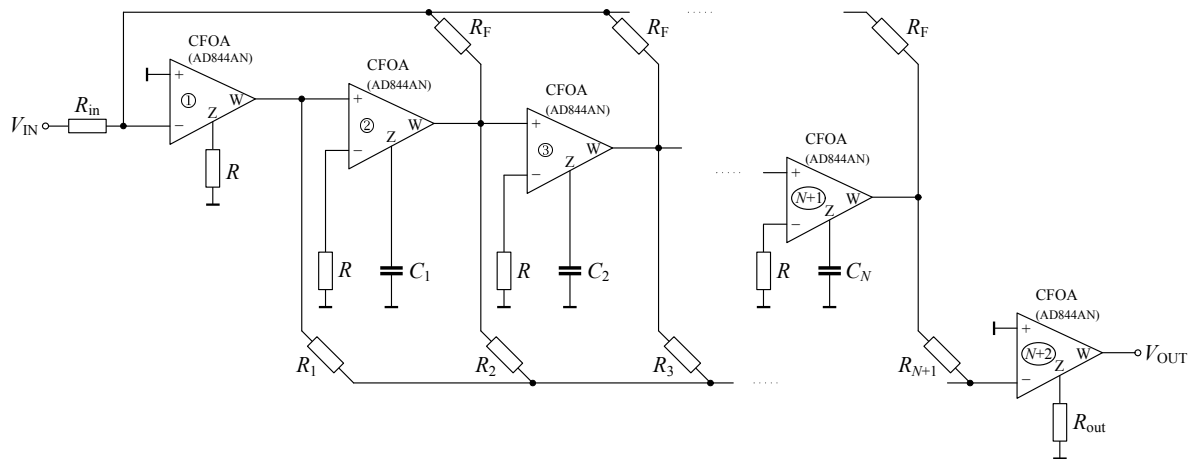


Figure 9. CFOA-based circuit to realize the proposed filters.

The transfer functions of the proposed filters, as given by (10)–(17), are chosen as demonstrative cases for circuit realization.

$$H_{FLPF}^{0.6,0.8,4}(s) = \frac{0.0010s^4 + 1.0608s^3 + 6.4002s^2 + 2.5499s + 0.0741}{s^4 + 11.0810s^3 + 15.1524s^2 + 3.2481s + 0.0770} \quad (10)$$

$$H_{FILPF}^{0.6,0.8,4}(s) = H_{FLPF}^{0.6,-0.8,4}(s) = \frac{1000s^4 + 11081s^3 + 15152.4s^2 + 3248.1s + 77}{s^4 + 1060.8s^3 + 6400.2s^2 + 2549.9s + 74.1} \quad (11)$$

$$H_{FHFP}^{0.8,0.5,4}(s) = \frac{0.9944s^4 + 19.1491s^3 + 24.7984s^2 + 2.2881s + 0.0056}{s^4 + 21.4372s^3 + 49.5967s^2 + 21.4372s + 1.0000} \quad (12)$$

$$H_{FIHFP}^{0.8,0.5,4}(s) = H_{FHFP}^{0.8,-0.5,4}(s) = \frac{1.0056s^4 + 21.5579s^3 + 49.8760s^2 + 21.5579s + 1.0056}{s^4 + 19.2569s^3 + 24.9381s^2 + 2.3010s + 0.0056} \quad (13)$$

$$H_{FBPF}^{0.65,0.85,4}(s) = \frac{0.0340s^4 + 6.8775s^3 + 71.8572s^2 + 6.8775s + 0.0340}{s^4 + 43.2076s^3 + 189.9142s^2 + 43.2076s + 1.0000} \quad (14)$$

$$H_{FIBPF}^{0.65,0.85,4}(s) = H_{FBPF}^{0.65,-0.85,4}(s) = \frac{29.4118s^4 + 1270.8s^3 + 5585.7s^2 + 1270.8s + 29.4118}{s^4 + 202.2794s^3 + 2113.4s^2 + 202.2794s + 1.0000} \quad (15)$$

$$H_{FBSF}^{0.75,0.65,4}(s) = \frac{0.9888s^4 + 21.8400s^3 + 31.5924s^2 + 21.8400s + 0.9888}{s^4 + 25.4992s^3 + 68.2322s^2 + 25.4992s + 1.0000} \quad (16)$$

$$H_{FIBSF}^{0.75,0.65,4}(s) = H_{FBSF}^{0.75,-0.65,4}(s) = \frac{1.0113s^4 + 25.7880s^3 + 69.0051s^2 + 25.7880s + 1.0113}{s^4 + 22.0874s^3 + 31.9502s^2 + 22.0874s + 1.0000} \quad (17)$$

The component values to realize the proposed filters, as shown in Table 12, considering a shift frequency of 1000 rad/s, are chosen from the industrial E24 and E12 series for the resistors and capacitors, respectively. The actual values of  $R_1$  and  $R_5$  for the FLPF and

FHPF are evaluated as 10 M $\Omega$  and 1.78 M $\Omega$ , respectively; for practical purposes, these values are set as  $\infty \Omega$  (i.e., open circuit). Circuit simulations are carried out in OrCAD PSPICE software with the AD844A/AD IC SPICE model used as the CFOA. The SPICE simulated magnitude and phase responses of the proposed filters are shown in Figure 10a,b; the same for their inverse functions are presented in Figure 11a,b. It is found that the frequency-domain behavior of the proposed filters designed using the nominal values of components attain good agreement with the theoretical characteristics. Quantitatively, the absolute maximum deviations in {magnitude, phase} of the designed FLPF, FILPF, FHPF, FIHPF, FBPF, FIBPF, FBSF, and FIBSF from the theoretical characteristics are {0.0374, 6.72 $^\circ$ }, {1.9915, 6.76 $^\circ$ }, {0.0360, 11.65 $^\circ$ }, {3.1215, 3.36 $^\circ$ }, {0.0170, 2.87 $^\circ$ }, {1.3074, 8.48 $^\circ$ }, {0.0633, 4.74 $^\circ$ }, and {0.1128, 5.76 $^\circ$ }, respectively. The ARME and ARPE indices with  $L = 100$  log-spaced data sample points, yielded for the SPICE-simulated filters based on the nominal values of passive components are presented in Table 13; in Figure 12a,b, the broken line graphs of these error indices for each design case are also presented.

Monte-Carlo simulations are conducted in PSPICE to determine the performance of the filters due to 5% and 10% deviations (following a Gaussian distribution) from the nominal values of resistors and capacitors, respectively. In total, 100 Monte-Carlo runs are carried out for each case and the magnitude and phase plots are shown in green in Figures 10 and 11. The minimum (min), max, mean, and standard deviation (SD) indices for the magnitude and phase at 1000 rad/s of the practical filters are presented in Table 14. The small values of SD justify good agreement with the theoretical (ideal) characteristics.

**Table 12.** Values of components to realize the proposed filters. [Note: Numbers in parenthesis represent  $(\alpha, \beta)$ ].

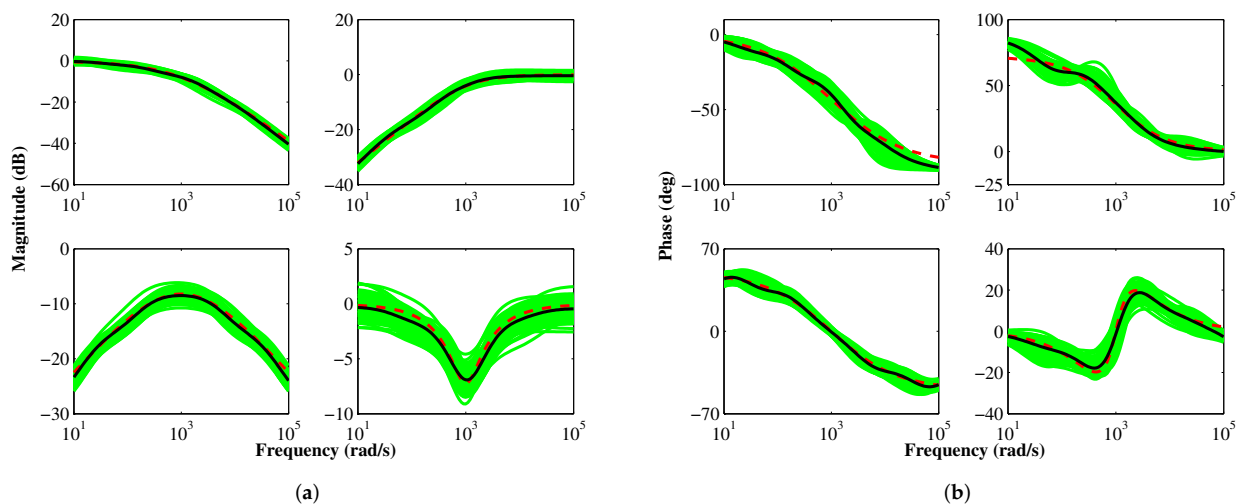
Component	FLPF (0.6, 0.8)	FILPF (0.6, 0.8)	FHPF (0.8, 0.5)	FIHPF (0.8, 0.5)	FBPF (0.65, 0.85)	FIBPF (0.65, 0.85)	FBSF (0.75, 0.65)	FIBSF (0.75, 0.65)
$R$ (k $\Omega$ )	10	100	10	100	7.5	100	75	100
$R_F$ (k $\Omega$ )	10	1	10	100	7.5	100	75	100
$R_{out}$ (k $\Omega$ )	10	100	10	11	7.5	10	75	110
$R_{in}$ (k $\Omega$ )	10	10	10	10	7.5	10	75	100
$R_1$ (k $\Omega$ )	$\infty$	1	10	100	220	3.3	75	100
$R_2$ (k $\Omega$ )	100	1	11	91	47	16	91	82
$R_3$ (k $\Omega$ )	24	4.3	20	51	20	39	160	47
$R_4$ (k $\Omega$ )	13	8.2	91	11	47	16	91	82
$R_5$ (k $\Omega$ )	10	10	$\infty$	0.56	220	3.3	75	100
$C_1$ (nF)	10	1	4.7	0.56	3.3	0.047	0.56	0.47
$C_2$ (nF)	68	1.8	47	8.2	33	1	4.7	6.8
$C_3$ (nF)	470	27	220	100	560	100	33	15
$C_4$ ( $\mu$ F)	3.9	0.33	2.2	3.9	5.6	2.2	0.33	0.22

**Table 13.** ARME and ARPE performances of the SPICE-simulated proposed filters based on nominal values of components.

Metric	Index	FLPF (0.6, 0.8)	FILPF (0.6, 0.8)	FHPF (0.8, 0.5)	FIHPF (0.8, 0.5)	FBPF (0.65, 0.85)	FIBPF (0.65, 0.85)	FBSF (0.75, 0.65)	FIBSF (0.75, 0.65)
ARME (dB)	Max	−15.84	−15.52	−20.50	−22.19	−16.05	−16.66	−22.85	−23.72
	Mean	−27.80	−22.10	−30.05	−29.94	−28.24	−24.11	−26.94	−31.91
ARPE (dB)	Max	−11.77	−11.32	−0.56	7.88	−8.07	2.90	6.97	8.67
	Mean	−21.61	−20.20	−15.92	−14.56	−26.31	−16.47	−12.57	−12.87

**Table 14.** Statistical indices about the magnitude/phase at the shift frequency of the designed filters based on 100 Monte-Carlo simulation runs.

Parameter @ 1 krad/s	Index	FLPF (0.6, 0.8)	FILPF (0.6, 0.8)	FHPF (0.8, 0.5)	FIHPF (0.8, 0.5)	FBPF (0.65, 0.85)	FIBPF (0.65, 0.85)	FBSF (0.75, 0.65)	FIBSF (0.75, 0.65)
Magnitude (dB)	Min	−10.56	5.60	−5.98	1.68	−10.75	5.99	−9.10	4.95
	Max	−6.22	9.79	−1.72	6.11	−6.18	10.15	−4.58	8.98
	Mean	−7.99	7.55	−4.05	3.78	−8.50	8.03	−6.88	7.08
	SD	0.932	0.921	0.972	0.962	0.898	0.851	0.902	0.850
	Ideal	−8.02	8.02	−4.18	4.18	−8.22	8.22	−7.25	7.25
Phase (deg)	Min	−52.42	34.16	31.03	−51.45	−4.19	−4.02	−14.24	−11.79
	Max	−31.51	54.64	49.47	−27.64	4.24	5.99	9.63	9.86
	Mean	−41.07	42.07	38.10	−36.59	−0.13	2.15	−1.07	−0.56
	SD	4.154	3.875	4.287	4.587	1.875	1.747	4.393	4.692
	Ideal	−43.20	43.20	36.00	−36.00	0.00	0.00	0.00	0.00

**Figure 10.** SPICE simulated (a) magnitude and (b) phase responses of the proposed FLPF, FHPF, FBPF, and FBSF. [Note: Theoretical responses are shown in dashed red; responses based on nominal values of components are shown in solid black; Monte-Carlo simulation-based responses are shown in green].

### 3.2.2. Experimental Validation

The hardware circuit realizations of the proposed FBPF and FIBPF, whose transfer functions are defined by (14) and (15), respectively, are demonstrated as representative cases in this section. The commercial Analog Devices AD844AN-type CFOAs were employed as the active elements. The ICs were provided with the supply voltage from the Agilent E3630A power supply. The OMICRON Lab Bode 100 network analyzer was used to measure the frequency response (magnitude and phase) of the practical filter circuits. The level of the testing harmonic signal was set to 1 V and 100 mV (peak-to-peak values) for the FBPF and FIBPF circuits, respectively. An Agilent InfiniVision DSO-X 2002A digital storage oscilloscope was used to observe the time-domain response of the filters. The FBPF and FIBPF circuits were subjected to a peak-to-peak signal of 1 V and 100 mV, respectively, from the Agilent 33521A function/arbitrary waveform generator. The photograph of the experimental set-up for the FIBPF is illustrated in Figure 13.

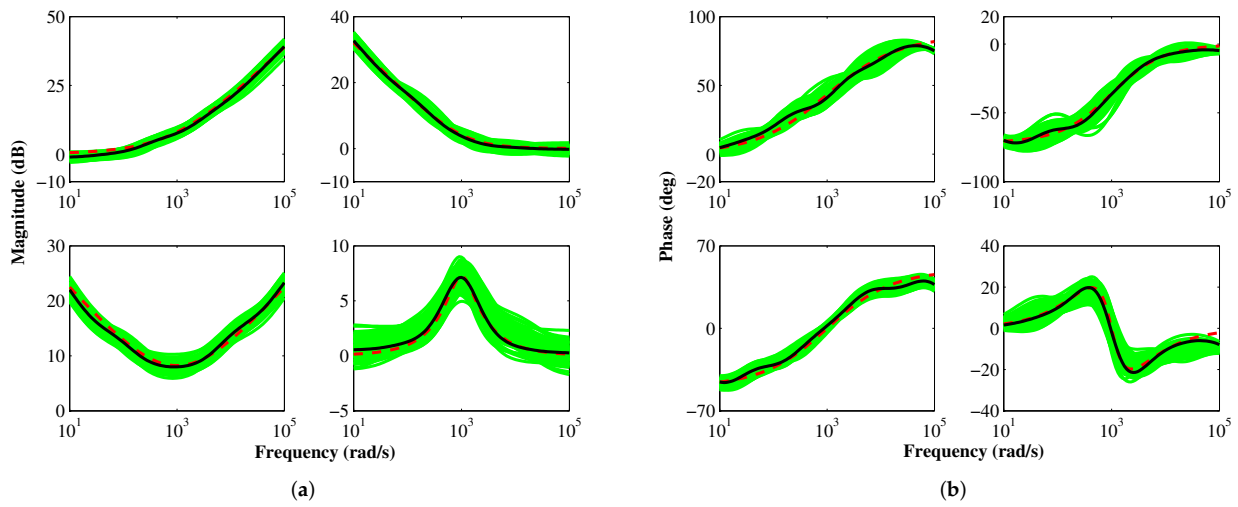


**Figure 11.** SPICE simulated (a) magnitude and (b) phase responses of the proposed FILPF, FIHPF, FIBPF, and FIBSF. [Note: Theoretical responses are shown in dashed red; responses based on nominal values of components are shown in solid black; Monte-Carlo simulation-based responses are shown in green].

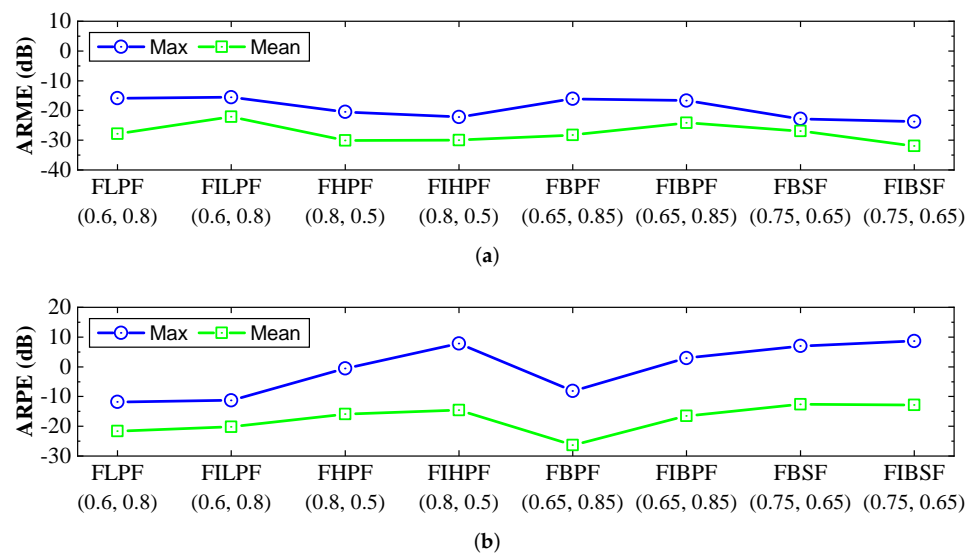


**Figure 12.** Broken line plots of the (a) ARME and (b) ARPE responses for the SPICE simulated proposed FLPF, FHPE, FBPE, FBSE, and their inverse counterparts realized using the nominal values of components.

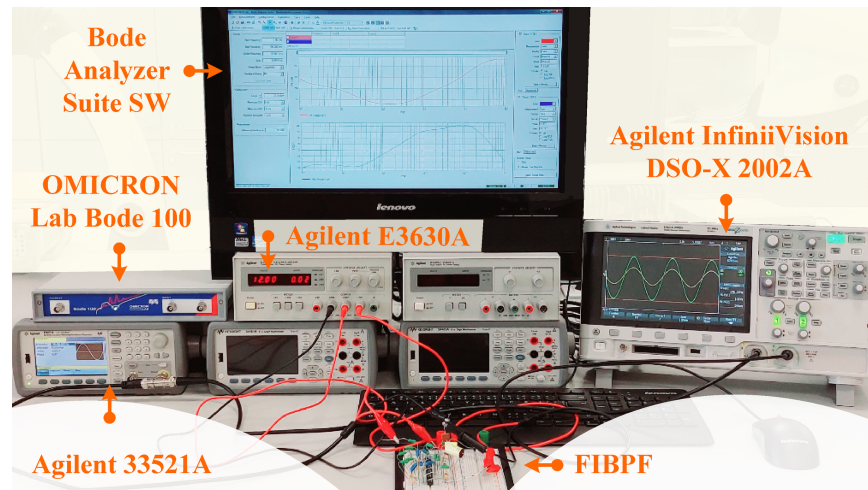


Figure 13. Photograph of the experimental set-up.

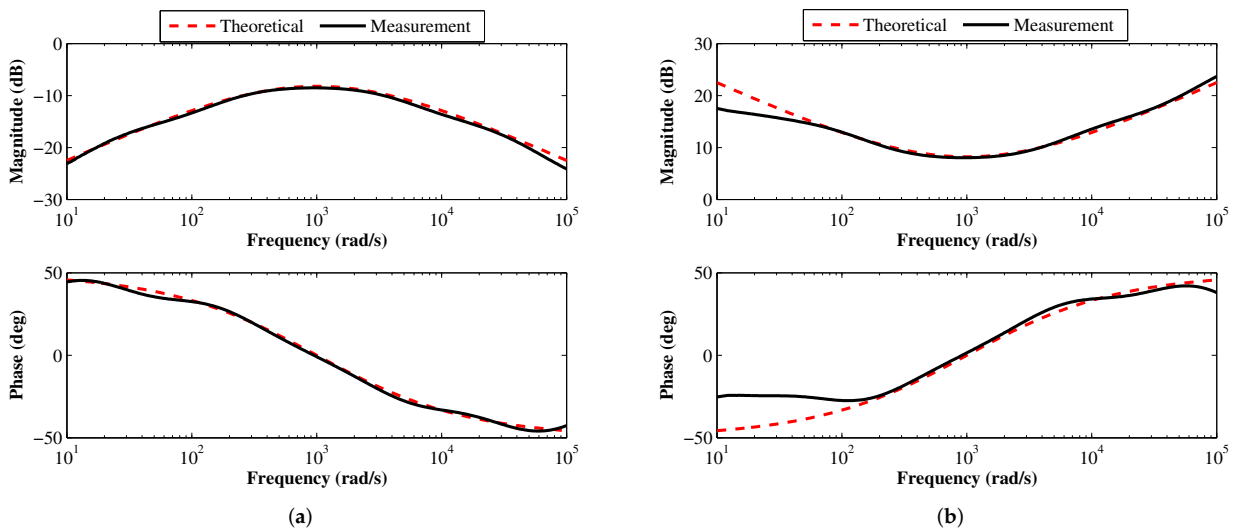
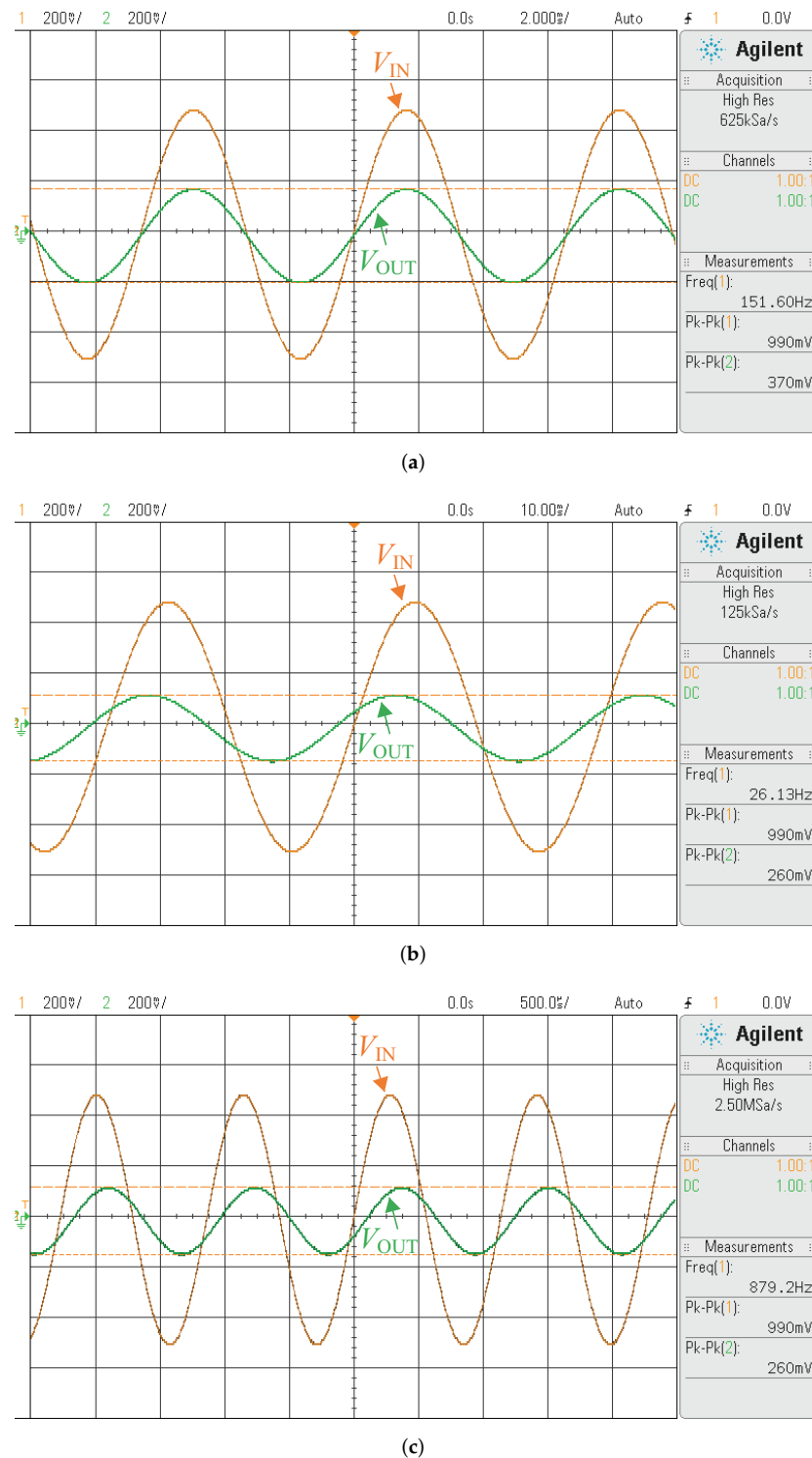


Figure 14. Magnitude and phase responses of the proposed (a) FBPF and (b) FIBPF based on experimental measurements.

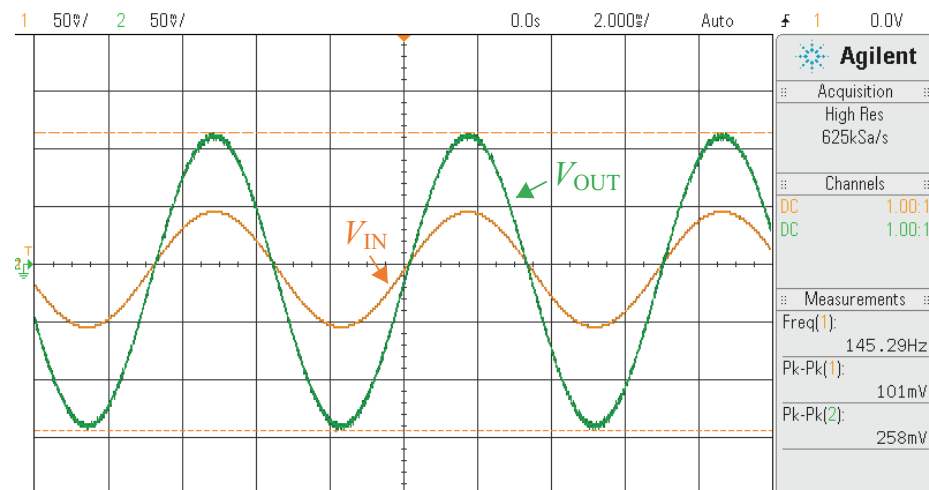
The experimentally measured magnitude and phase responses of the FBPF and FIBPF are presented in Figure 14a,b, respectively. Comparisons with the theoretical characteristics reveal that: (i) the {max ARME (dB), mean ARME (dB), max ARPE (dB), and mean ARPE (dB)} values for the FBPF and FIBPF are  $\{-15.19, -27.20, 5.82, -22.53\}$  and  $\{-7.28, -22.07, 10.54, -13.37\}$ , respectively; (ii) the responses of the FBPF stay in proximity to the theoretical plots throughout the design range; (iii) for the FIBPF, the magnitude and phase responses deviate from the theoretical ones in the frequency range  $[10, 48.49]$  rad/s and  $[10, 129]$  rad/s, respectively; (iv) the magnitude of the FBPF at the center frequency ( $\omega_0 = 952.53$  rad/s), lower half-power frequency ( $\omega_{H,low} = 164.18$  rad/s), and upper half-power frequency ( $\omega_{H,high} = 5.52$  krad/s) is  $-8.55$  dB,  $-11.61$  dB, and  $-11.61$  dB, respectively. The corresponding theoretical magnitude values at these frequencies are  $-8.22$  dB,  $-11.25$  dB, and  $-10.96$  dB; and (v) the magnitude at  $\omega_0$  ( $=912.44$  rad/s),  $\omega_{H,low}$  ( $=171.53$  rad/s), and  $\omega_{H,high}$  ( $=5.26$  krad/s) for the theoretical FIBPF is 8.23 dB, 11.12 dB, and 10.81 dB, respectively. The corresponding measured values from the practical filter are 8.14 dB, 10.96 dB, and 11.13 dB, which demonstrate closeness with the theoretical anticipations.

Figure 15a–c present the time-domain response measurements of the FBPF when the input signal frequency is  $\omega_0$ ,  $\omega_{H,low}$ , and  $\omega_{H,high}$ , respectively. The peak-to-peak output voltage ( $V_{OUT,P-P}$ ) for these considered cases is obtained as 370 mV, 260 mV, and 260 mV,

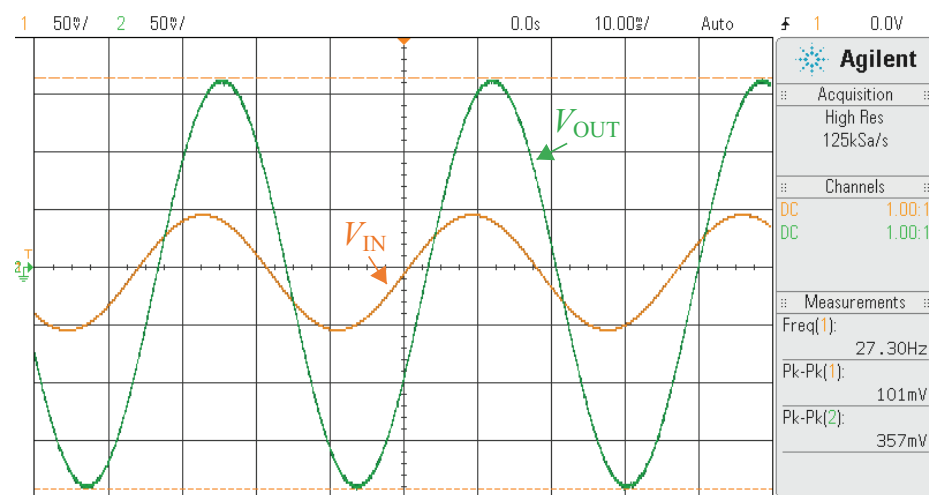
respectively, which matches closely with the theoretical values of 384.27 mV, 271.10 mV, and 280.30 mV. The time-domain waveforms of the FIBPF for these same frequencies are illustrated in Figure 16a–c. It is found that  $V_{OUT,P-P}$  of 258 mV, 357 mV, and 364 mV is yielded by the practical filter, which agrees with the theoretical values of 260.51 mV, 363.34 mV, and 350.61 mV, at the excitation frequencies  $\omega_0$ ,  $\omega_{H,low}$ , and  $\omega_{H,high}$ , respectively.



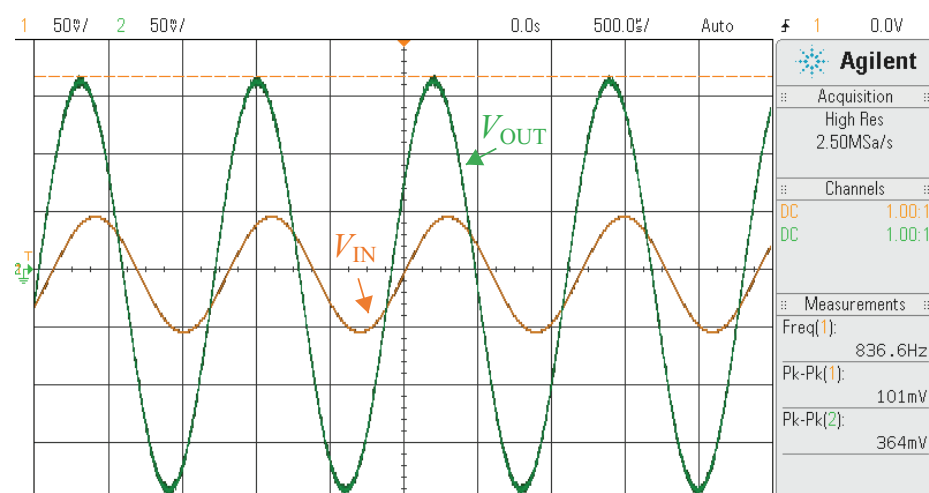
**Figure 15.** Time-domain input-output waveforms observed in oscilloscope for the proposed FIBPF with an input frequency of (a)  $\omega_0 = 952.53$  rad/s, (b)  $\omega_{H,low} = 164.18$  rad/s, and (c)  $\omega_{H,high} = 5.52$  krad/s.



(a)



(b)



(c)

**Figure 16.** Time-domain input-output waveforms observed in oscilloscope for the proposed FIBPF with an input frequency of (a)  $\omega_0 = 912.44$  rad/s, (b)  $\omega_{H,low} = 171.53$  rad/s, and (c)  $\omega_{H,high} = 5.26$  krad/s.

In Figure 17a–c, the Fast Fourier Transform spectrum measurements displayed up to the sixth harmonic above  $-92$  dBV of the FBPF at  $\omega_0$ ,  $\omega_{H,low}$ , and  $\omega_{H,high}$ , are presented. The Spurious-Free Dynamic Range (SFDR) for these three cases are obtained as 54.80 dBc, 51.12 dBc, and 54.63 dBc, respectively; the Total Harmonic Distortion (THD) is determined from the first six harmonics as 0.25%, 0.34%, and 0.29%, respectively. The experimentally obtained Fourier spectrums up to the sixth harmonic above  $-92$  dBV for the FIBPF at frequencies of  $\omega_0$ ,  $\omega_{H,low}$ , and  $\omega_{H,high}$  are shown in Figure 18a–c. Experimental results reveal that the {SFDR, THD} for these three cases are {68.40 dBc, 0.06%}, {58.40 dBc, 0.17%}, and {57.73 dBc, 0.16%}, respectively.

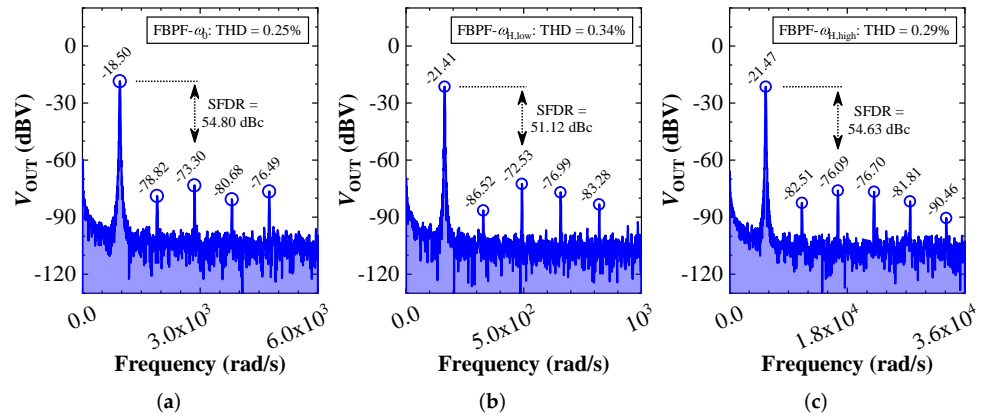


**Figure 17.** Experimentally obtained Fourier spectrums of the proposed FBPF at frequency of (a)  $\omega_0 = 952.53$  rad/s, (b)  $\omega_{H,low} = 164.18$  rad/s, and (c)  $\omega_{H,high} = 5.52$  krad/s.

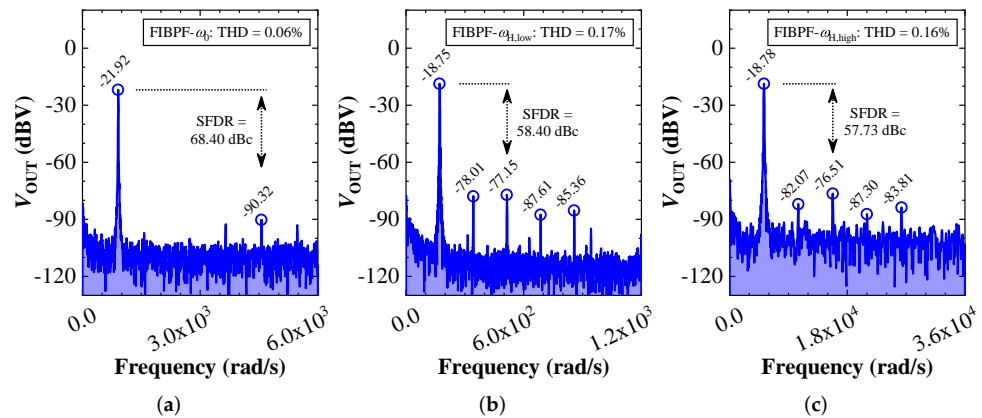


**Figure 18.** Experimentally obtained Fourier spectrums of the proposed FIBPF at frequency of (a)  $\omega_0 = 912.44$  rad/s, (b)  $\omega_{H,low} = 171.53$  rad/s, and (c)  $\omega_{H,high} = 5.26$  krad/s.

#### 4. Conclusions

Further generalization of the fractional-order filters exhibiting the low-pass, high-pass, band-pass, and band-stop behavior of the second-order limiting form is presented along with their optimal and stable rational approximation in this paper. It is demonstrated that the power-law filters [20–23] can be treated as a particular case of the proposed filters, since the proposed model introduces an additional degree-of-freedom (viz. the new tuning parameter  $\alpha$ ) in the transfer function of the power-law filter. A different approach is adopted to formulate the design constraints compared to the published literature [21]. The proposed strategy also allows the attainment of stable inverse filters since the zeros and poles of the approximant pertaining to the standard filter are constrained to lie in the left-half  $s$ -plane.

The performance of the proposed models in approximating the frequency-domain characteristics of the theoretical filter is investigated using different error indices. Cur-

rent feedback operational amplifiers are employed as active components to realize the discrete components based circuits for the proposed filters and their inverse counterparts. Monte-Carlo simulations conducted in SPICE environment highlight good agreement in the magnitude and phase responses of the designed models with the theory. Hardware implementations of the proposed fractional-order band-pass (both normal and inverse) filters and their magnitude-frequency, phase-frequency, AC transients, and Fourier analysis are also presented to demonstrate the practical viability.

Future work will investigate the effectiveness of the proposed transfer function in improving the design performances of the power law compensator [45] and the bioimpedance models [46].

**Author Contributions:** Conceptualization, S.M. and N.H.; methodology, S.M.; software, S.M.; validation, S.M., N.H., and D.K.; formal analysis, S.M.; investigation, S.M.; resources, N.H.; data curation, S.M.; writing—original draft preparation, S.M. and N.H.; writing—review and editing, S.M., N.H., and D.K.; visualization, S.M. and N.H.; supervision, N.H.; project administration, N.H.; funding acquisition, N.H. All authors have read and agreed to the published version of the manuscript.

**Funding:** The research results described in this paper are supported by The Czech Science Foundation, project No. 19-24585S.

**Institutional Review Board Statement:** Not applicable.

**Informed Consent Statement:** Not applicable.

**Data Availability Statement:** All the data are presented in the paper.

**Conflicts of Interest:** The authors declare no conflicts of interest.

## Abbreviations

The following abbreviations are used in this manuscript:

ARME	Absolute relative magnitude error
ARPE	Absolute relative phase error
BP	Band-pass
BS	Band-stop
CFOA	Current feedback operational amplifier
C <sup>2</sup> oDE	Constrained composite differential evolution
FBPF	Fractional-order band-pass filter
FBSF	Fractional-order band-stop filter
FHPF	Fractional-order high-pass filter
FIBPF	Fractional-order inverse band-pass filter
FIBSF	Fractional-order inverse band-stop filter
FIHPF	Fractional-order inverse high-pass filter
FILPF	Fractional-order inverse low-pass filter
FLPF	Fractional-order low-pass filter
FO	Fractional-order
FTF	Fractional-order transfer function
HP	High-pass
ITF	Integer-order transfer function
LP	Low-pass
PLF	Power-law filter
SD	Standard deviation
SFDR	Spurious-free dynamic range
SPICE	Simulation program with integrated circuit emphasis
THD	Total harmonic distortion

## References

1. Monje, C.A.; Chen, Y.; Vinagre, B.M.; Xue, D.; Feliu-Batlle, V. *Fractional-Order Systems and Controls: Fundamentals and Applications*; Springer Science & Business Media: Berlin/Heidelberg, Germany, 2010.
2. Sun, H.; Zhang, Y.; Baleanu, D.; Chen, W.; Chen, Y. A new collection of real world applications of fractional calculus in science and engineering. *Commun. Nonlinear Sci. Numer. Simul.* **2018**, *64*, 213–231. [[CrossRef](#)]
3. Elwakil, A.S. Fractional-order circuits and systems: An emerging interdisciplinary research area. *IEEE Circuits Syst. Mag.* **2010**, *10*, 40–50. [[CrossRef](#)]
4. Hélie, T. Simulation of fractional-order low-pass filters. *IEEE/ACM Trans. Audio Speech Lang. Process.* **2014**, *22*, 1636–1647. [[CrossRef](#)]
5. Kubanek, D.; Freeborn, T.; Koton, J. Fractional-order band-pass filter design using fractional-characteristic specimen functions. *Microelectron. J.* **2019**, *86*, 77–86. [[CrossRef](#)]
6. Acharya, A.; Das, S.; Pan, I.; Das, S. Extending the concept of analog Butterworth filter for fractional order systems. *Signal Process.* **2014**, *94*, 409–420. [[CrossRef](#)]
7. AbdelAty, A.M.; Soltan, A.; Ahmed, W.A.; Radwan, A.G. Fractional order Chebyshev-like low-pass filters based on integer order poles. *Microelectron. J.* **2019**, *90*, 72–81. [[CrossRef](#)]
8. Varshney, G.; Pandey, N.; Pandey, R. Generalization of shadow filters in fractional domain. *Int. J. Circuit Theor. Appl.* **2021**, *49*, 3248–3265. [[CrossRef](#)]
9. Adhikary, A.; Sen, S.; Biswas, K. Design and hardware realization of a tunable fractional-order series resonator with high quality factor. *Circuits Syst. Signal Process.* **2017**, *36*, 3457–3476. [[CrossRef](#)]
10. Soltan, A.; Radwan, A.G.; Soliman, A.M. Fractional order Sallen–Key and KHN filters: Stability and poles allocation. *Circuits Syst. Signal Process.* **2015**, *34*, 1461–1480. [[CrossRef](#)]
11. Bertsias, P.; Psychalinos, C.; Elwakil, A.S.; Biswas, K. Single transistor fractional-order filter using a multi-walled carbon nanotube device. *Analog Integr. Circuits Signal Process.* **2019**, *100*, 215–219. [[CrossRef](#)]
12. Biswas, K.; Bohannan, G.; Caponetto, R.; Lopes, A.M.; Machado, J.A.T. *Fractional-Order Devices*; Springer: Berlin/Heidelberg, Germany, 2017.
13. Freeborn, T.J. Comparison of  $(1 + \alpha)$  fractional-order transfer functions to approximate lowpass Butterworth magnitude responses. *Circuits Syst. Signal Process.* **2016**, *35*, 1983–2002. [[CrossRef](#)]
14. Mahata, S.; Kar, R.; Mandal, D. Optimal modelling of  $(1 + \alpha)$  order Butterworth filter under the CFE framework. *Fractal Fract.* **2020**, *4*, 55. [[CrossRef](#)]
15. Mijat, N.; Jurisic, D.; Moschytz, G.S. Analog modeling of fractional-order elements: A classical circuit theory approach. *IEEE Access* **2021**, *9*, 110309–110331. [[CrossRef](#)]
16. Valsa, J.; Vlach, J. RC models of a constant phase element. *Int. J. Circuit Theor. Appl.* **2013**, *41*, 59–67. [[CrossRef](#)]
17. Colín-Cervantes, J.D.; Sánchez-López, C.; Ochoa-Montiel, R.; Torres-Muñoz, D.; Hernández-Mejía, C.M.; Sánchez-Gaspariano, L.A.; González-Hernández, H.G. Rational approximations of arbitrary order: A survey. *Fractal Fract.* **2021**, *5*, 267. [[CrossRef](#)]
18. Langhammer, L.; Dvorak, J.; Jerabek, J.; Koton, J.; Sotner, R. Fractional-order low-pass filter with electronic tunability of its order and pole frequency. *J. Electr. Eng.* **2018**, *69*, 3–13. [[CrossRef](#)]
19. Mahata, S.; Herencsar, N.; Kubanek, D.; Kar, R.; Mandal, D.; Goknar, C.I. A fractional-order transitional Butterworth-Butterworth filter and its experimental validation. *IEEE Access* **2021**, *9*, 129521–129527. [[CrossRef](#)]
20. Kapoulea, S.; Psychalinos, C.; Elwakil, A.S. Power law filters: A new class of fractional-order filters without a fractional-order Laplacian operator. *AEU-Int. J. Electron. Commun.* **2021**, *129*, 153537. [[CrossRef](#)]
21. Mahata, S.; Herencsar, N.; Kubanek, D. On the design of power law filters and their inverse counterparts. *Fractal Fract.* **2021**, *5*, 197. [[CrossRef](#)]
22. Tsouvalas, E.; Kapoulea, S.; Psychalinos, C.; Elwakil, A.S.; Jurišić, D. Electronically controlled power-law filters realizations. *Fractal Fract.* **2022**, *6*, 111. [[CrossRef](#)]
23. Kapoulea, S.; Psychalinos, C.; Elwakil, A.S. Versatile field-programmable analog array realizations of power-law filters. *Electronics* **2022**, *11*, 692. [[CrossRef](#)]
24. Radwan, A.G.; Elwakil, A.S.; Soliman, A.M. On the generalization of second-order filters to the fractional-order domain. *J. Circuits Syst. Comput.* **2009**, *18*, 361–386. [[CrossRef](#)]
25. Said, L.A.; Ismail, S.M.; Radwan, A.G.; Madian, A.H.; El-Yazeed, M.F.A.; Soliman, A.M. On the optimization of fractional order low-pass filters. *Circuits Syst. Signal Process.* **2016**, *35*, 2017–2039. [[CrossRef](#)]
26. Kubanek, D.; Freeborn, T.  $(1+\alpha)$  fractional-order transfer functions to approximate low-pass magnitude responses with arbitrary quality factor. *AEU-Int. J. Electron. Commun.* **2018**, *83*, 570–578. [[CrossRef](#)]
27. Mahata, S.; Saha, S.; Kar, R.; Mandal, D. Optimal integer-order rational approximation of  $\alpha$  and  $\alpha + \beta$  fractional-order generalised analogue filters. *IET Signal Process.* **2019**, *13*, 516–527. [[CrossRef](#)]
28. Kapoulea, S.; Psychalinos, C.; Elwakil, A.S. Double exponent fractional-order filters: Approximation methods and realization. *Circuits Syst. Signal Process.* **2021**, *40*, 993–1004. [[CrossRef](#)]
29. Mohapatra, A.S.; Biswas, K. A fractional order notch filter to compensate the attenuation-loss due to change in order of the circuit. *IEEE Trans. Circuits Syst. I Regul. Pap.* **2020**, *68*, 655–666. [[CrossRef](#)]

30. AbdelAty, A.M.; Fouda, M.E.; Elbarawy, M.T.M.M.; Radwan, A.G. Optimal charging of fractional-order circuits with cuckoo search. *J. Adv. Res.* **2021**, *32*, 119–131. [[CrossRef](#)]
31. Wang, B.C.; Li, H.X.; Li, J.P.; Wang, Y. Composite differential evolution for constrained evolutionary optimization. *IEEE Trans. Syst. Man Cybern. Syst.* **2018**, *49*, 1482–1495. [[CrossRef](#)]
32. Wang, Y.; Cai, Z.; Zhang, Q. Differential evolution with composite trial vector generation strategies and control parameters. *IEEE Trans. Evol. Comput.* **2011**, *15*, 55–66. [[CrossRef](#)]
33. Deb, K. An efficient constraint handling method for genetic algorithms. *Comput. Methods Appl. Mech. Eng.* **2000**, *186*, 311–338. [[CrossRef](#)]
34. Takahama, T.; Sakai, S. Constrained optimization by the  $\epsilon$  constrained differential evolution with an archive and gradient-based mutation. In Proceedings of the IEEE Congress on Evolutionary Computation, Barcelona, Spain, 18–23 July 2010; pp. 1–9. [[CrossRef](#)]
35. Senani, R.; Bhaskar, D.R.; Raj, A. Inverse analog filters: History, progress and unresolved issues. *Electronics* **2022**, *11*, 841. [[CrossRef](#)]
36. Bhaskar, D.R.; Kumar, M.; Kumar, P. Fractional order inverse filters using operational amplifier. *Analog Integr. Circuits Signal Process.* **2018**, *97*, 149–158. [[CrossRef](#)]
37. Khalil, N.A.; Said, L.A.; Radwan, A.G.; Soliman, A.M. Multifunction fractional inverse filter based on OTRA. In Proceedings of the 2019 Novel Intelligent and Leading Emerging Sciences Conference (NILES), Giza, Egypt, 28–30 October 2019; Volume 1, pp. 162–165. [[CrossRef](#)]
38. Bertias, P.; Tsirimokou, G.; Psychalinos, C.; Elwakil, A.S. Fully electronically tunable inverse fractional-order filter designs. In Proceedings of the 2019 Novel Intelligent and Leading Emerging Sciences Conference (NILES), Giza, Egypt, 28–30 October 2019; Volume 1, pp. 42–45. [[CrossRef](#)]
39. Hamed, E.M.; Said, L.A.; Madian, A.H.; Radwan, A.G. On the approximations of CFOA-based fractional-order inverse filters. *Circuits Syst. Signal Process.* **2020**, *39*, 2–29. [[CrossRef](#)]
40. Srivastava, J.; Bhagat, R.; Kumar, P. Analog inverse filters using OTAs. In Proceedings of the 2020 6th International Conference on Control, Automation and Robotics (ICCAR), Singapore, 20–23 April 2020; pp. 627–631. [[CrossRef](#)]
41. Bhaskar, D.R.; Kumar, M.; Kumar, P. Minimal realization of fractional-order inverse filters. *IETE J. Res.* **2020**, 1–14. [[CrossRef](#)]
42. Paarmann, L.D. *Design and Analysis of Analog Filters: A Signal Processing Perspective*; Springer Science & Business Media: Berlin/Heidelberg, Germany, 2006; Volume 617.
43. Muñoz-Montero, C.; García-Jiménez, L.V.; Sánchez-Gaspariano, L.A.; Sánchez-López, C.; González-Díaz, V.R.; Tlelo-Cuautle, E. New alternatives for analog implementation of fractional-order integrators, differentiators and PID controllers based on integer-order integrators. *Nonlinear Dyn.* **2017**, *90*, 241–256. [[CrossRef](#)]
44. Senani, R.; Bhaskar, D.R.; Singh, A.K.; Singh, V.K. *Current Feedback Operational Amplifiers and Their Applications*; Springer: Berlin/Heidelberg, Germany, 2013.
45. Kapoulea, S.; Psychalinos, C.; Elwakil, A.S.; Tavazoei, M.S. Power-law compensator design for plants with uncertainties: Experimental verification. *Electronics* **2021**, *10*, 1305. [[CrossRef](#)]
46. Kapoulea, S.; Elwakil, A.S.; Psychalinos, C.; Al-Ali, A. Novel double-dispersion models based on power-law filters. *Circuits Syst. Signal Process.* **2021**, *40*, 5799–5812. [[CrossRef](#)]